

REPORT DOCUMENTATION PAGE			Form Approved OMB No. 0704-0188	
Public reporting burden for this collection of information is estimated to average 1 hour per response, including the time for reviewing instructions, searching existing data sources, gathering and maintaining the data needed, and completing and reviewing the collection of information. Send comments regarding this burden estimate or any other aspect of this collection of information, including suggestions for reducing this burden, to Washington Headquarters Services, Directorate for Information Operations and Reports, 1215 Jefferson Davis Highway, Suite 1204, Arlington, VA 22202-4302, and to the Office of Management and Budget, Paperwork Reduction Project (0704-0188), Washington, DC 20503.				
1. AGENCY USE ONLY (Leave blank)	2. REPORT DATE	3. REPORT TYPE AND DATES COVERED		
	30 Jan 98	Final	15 Jan 95 - 14 Jul 97	
4. TITLE AND SUBTITLE			5. FUNDING NUMBERS	
"Synthesis, Interface and Properties of Nanodispersed Aluminum Alloys"			G - F49620-95-1-0105	
6. AUTHOR(S)				
Professor K. Chattopadhyay				
7. PERFORMING ORGANIZATION NAME(S) AND ADDRESS(ES)			8. PERFORMING ORGANIZATION REPORT NUMBER	
Indian Institute of Science Bangalore 560 012 India			N/A	
9. SPONSORING/MONITORING AGENCY NAME(S) AND ADDRESS(ES)			10. SPONSORING/MONITORING AGENCY REPORT NUMBER	
Asian Office of Aerospace Research and Development (AOARD) Unit 45002 APO AP 96337-5002			AOARD 95-01	
11. SUPPLEMENTARY NOTES				
19980521 129				
12a. DISTRIBUTION AVAILABILITY STATEMENT				
Approved for public release; distribution is unlimited.				
13. ABSTRACT (Maximum 200 words)				
<p>The work on synthesis and study of phase transformation of the soft phase dispersed in aluminum based matrices was obtained. This research successfully synthesized nanometric dispersions of bismuth (Bi) in a glassy Aluminum-Iron-Silicon (Al-Fe-Si) matrix by using rapid solidification technique. The Bi melt is immiscible with the ternary melt of Al-Fe-Si and phase separates. Thus quenching rapidly through the miscibility gap has enabled to obtain nanometric dispersions of Bi Particles in a glassy matrix. The final result also showed a large depression of the melting point when the sample was recycled in the differential scanning calorimeter (DSC). The depression of the melting point is reversible in nature by cycling the sample from few degrees above the depressed melting point.</p>				
<b>DTIC QUALITY INSPECTED</b>				
14. SUBJECT TERMS			15. NUMBER OF PAGES	
Synthesis, phase transformation, aluminum, nonometric, differential scanning calorimeter, quenching			56	
			16. PRICE CODE	
17. SECURITY CLASSIFICATION OF REPORT	18. SECURITY CLASSIFICATION OF THIS PAGE	19. SECURITY CLASSIFICATION OF ABSTRACT	20. LIMITATION OF ABSTRACT	
UNCLASSIFIED	UNCLASSIFIED	UNCLASSIFIED	UL	

# Final Report

## Synthesis, Interface and Properties of Nanodispersed Aluminum Alloys

**Principal Investigator: Professor K.Chattopadhyay**

### **Objective:**

The objectives of the original proposal were three fold. First, it aims at synthesizing aluminum-based nanomaterials with soft metallic and intermetallic dispersion. Following successful completion of this stage, detailed phase transformation studies of the soft phases was planned. In the last phase, studies on the mechanical behavior of the aluminum nanoalloys with intermetallic phase dispersions were planned to evaluate the possibility of developing new generation rapidly solidifies alloys. As the present report shows, within the constraint of time and resources, the objectives are met to a large extent.

### **Report on research accomplishments and new findings:**

#### **I. Soft dispersion in aluminum alloys**

The work on synthesis and study of phase transformation of the soft phase dispersed in aluminum based matrices has registered considerable success. We have able to successfully synthesize nanometric dispersions of Bi in a glassy Al-Fe-Si matrix by using rapid solidification technique. The Bi melt is immiscible with the ternary melt of Al-Fe-Si and phase separates. Thus quenching rapidly through the miscibility gap has enabled us to obtain nanometric dispersions of Bi particles in a glassy matrix. Bi melts below the

glass transition temperature of the glassy matrix and thus presents opportunities for the study of the melting and solidification behavior of the nanosolids under constraints.

The most striking result is the observation of a large depression of the melting point when the sample is recycled in the DSC. The depression of the melting point is reversible in nature in the sense that we can recover the depressed peak by cycling the sample from few degrees above the depressed melting point. Electron microscopic studies indicate that most of the Bi particles are originally single crystals. However, after cycling, the small particles show sectorial contrast indicating that they now contain multiple crystal domains. Our results suggest that any pressure effects cannot explain the depression of the melting point and represent a new finding. It is clearly related to the appearance of the above domains. However, further work is needed to establish the reason for this depression. The work appeared in Applied Physics Letter and is appended in the report (Annexure 1.1). During the project period, the principle investigator is also involved in writing a major review on superheating and melting of embedded nanoparticles, which will appear in the Progress in Materials Science (See Annexure 1.2).

## **II. Synthesis of Multiphase nanomaterials based on aluminum matrix by rapid solidification**

Nanostructured multiphase aluminum alloys with intermetallic second phase have potential for high strength application. The group led by the Prof. Inoue of Tohoku University, Sendai, Japan, has already shown that such dispersions in metallic glass matrix yield one of the highest specific strength materials. Unfortunately, however, the

glassy matrix is not very stable. Considerable work has been carried out on crystalline two-phase materials with micron sized grains primarily to utilize the superplastic behavior. In these cases, the inherent two-phase fine microstructure promotes superplasticity at an elevated temperature due to the sliding of the grains. The major goal was to develop a high strength alloy with easy formability as well as one that resists coarsening, simultaneously. The stable microstructures in these cases were achieved by secondary processing like recrystallisation and alloying additions.

It is in principle possible to produce nanostructured aluminum alloys by rapid solidification. It is well known that the additions of the rare earths and transition metals (eg. Zr) yield metallic glass in aluminum based systems. We argued that addition of these alloying additions in an amount slightly less than that needed for the glass formation will promote the nucleation of the intermetallic phase at an undercooled temperature and yield nanoscaled microstructure. Further the stability of the microstructure will depend on the nature of the partitioning of the ternary elements and the interdiffusivity of these elements. Thus a window may exist where such microstructure will be stable and provide us opportunity to develop a high strength material with high temperature superplastic properties.

With these in mind, we have tried to obtain a fine grained microstructure in some of the binary eutectics in Al based alloys in a single step process of rapid solidification with the addition of ternary elements. The ternary addition plays a role in effecting fine sizes of both the equilibrium phases under rapid quenching condition and later precipitates out as

the set up was ready this was mounted on to grips by a pin arrangement on to the Instron machine to lie centrally aligned. Just before the experiment began, the paper fixture was cut along premarked lines (as shown by dotted lines in the schematic) to expose the free sample to the load. A similar arrangement was designed in the high temperature metallic fixtures as well, so as to enable monitoring of the load on the sample alone.

Tensile testing was carried out at two slightly varying strain rates ( $2 \times 10^{-2} \text{ s}^{-1}$  and  $4 \times 10^{-2} \text{ s}^{-1}$ ). These were the instantaneous strain rates, the variable experimental parameter being the crosshead speed of the Instron machine (varied as  $3 \mu\text{m/s}$  and  $6 \mu\text{m/s}$ , respectively). The furnace was well calibrated within the three zones and the sample was adjusted to lie exactly at the center of the middle zone during the high temperature experiments. The fracture surfaces (ribbon cross section) were examined in the SEM.

#### **A. The near eutectic composition ( $\text{Al}_{82}\text{Cu}_{15}\text{Zr}_3$ )**

(i) **Microstructure:** The as spun microstructure comprises of two predominantly occurring regions. (a) One with  $\sim 1/2 \mu\text{m}$  grains of Al solid solution (Fig. 2a) with both solutes of Cu and Zr, and (b) an equiaxed microstructure comprising of both the binary eutectic phases Al and  $\text{Al}_2\text{Cu}$  in extremely fine sizes (Fig. 2b). Diffraction patterns from these regions reveal single crystal Al zones (Fig. 2c) and polycrystalline rings from both Al and  $\text{Al}_2\text{Cu}$  respectively (Fig. 2d). Both types of regions do not show any Zr containing compound and the ternary element is present in solution in both types of microstructures. This alloy displayed a microhardness of 400 VHN, as shown in a comparative plot in Fig.

**(ii) Thermal Stability:** The thermal stability of this alloy was examined at short times of 1 h at temperatures of 200 C, 300 C, 400 C and 500 C, as well as at a longer time of 8h at 400 C ( close to 3/4 ths the melting temperature of the Al matrix). Fig. 4 compares the heat treated microstructures (400 C 1 h, 500 C 1 h and 400 C 8 h, in the order Fig. 4 (a-c). On heat treatment, the individual grain structure is not so evident and they appear more as interconnected phases. Apart from grain growth, heat treatment also results in a phase transformation as evident from the fine structure seen within the grains of the heat treated samples. The third phase has been confirmed by using diffraction analysis in the TEM to be the  $L1_2$  compound  $Al_3Zr$ , a metastable phase, the equilibrium phase being one with a tetragonal structure. This phase can be seen in greater prominence with longer heat treatment times. At longer time at the lower temperatures as well as at higher temperatures, of 673 K and 773 K, the stable equilibrium tetragonal phase is also found alongwith the metastable phase (arowed). Although coarsening and phase transformation has occurred, this refers to only the Al grains and TEM evidence reveals that the precipitate phases still remain nanoscaled. A brief report of the microstructure evolution has been presented in the International Conference on Superplasticity and is published in Materials Science Forum (see Annexure 1.3).

**(iii) Mechanical Testing:** Room temperature testing revealed that this sample did not have too much of ductility as shown in a typical load Vs time curve plotted at a cross head speed of 3  $\mu\text{m/s}$  (Fig.5), the breaking stress occurring at 350 MPa, (gauge length = 15mm, cross section =  $40 \times 10^{-6} \text{mm}^2$  ). Several tests were made on the sample to check the reproducibility. This is tabulated table 1. The failing loads ranged from values as low

a fine intermetallic phase on heat treatment, which further enhances the stability to coarsening of the microstructure.

Zirconium has been found to be very effective in this regard. In smaller amount it is also a good grain refiner in Al castings. In addition it exhibits very low values of solubility and diffusivity in Al. We have studied three binary systems Al-Ni, Al-Cu and Al-Si with Zr as the alloying additions (ranging from 1 to 3 at. percent). All the alloys are of hypoeutectic compositions. All of them yield a nanoscaled microstructure on rapid solidification. However detailed microstructural studies using both the optical, scanning and transmission electron microscopes were carried out only on two systems containing Ni and Cu.

For initial studies of the mechanical properties, we have used the as spun ribbon of Al-Cu samples. Unfortunately it is extremely difficult to obtain the defect free continuous ribbons which complicates the data. The mechanical properties were tested at both room temperature and high temperatures using a screw driven Instron machine. Samples for mechanical testing were prepared and handled with great care. Separate special low load cells were fabricated to suit the load sensitivity of the thin ribbons (ranging from 0-10 Kg and 0 - 50 Kg, i.e. 100N and 500N respectively). Separate fixtures were made for the testing at high temperatures. At room temperature, initially the tests were carried out using cardboard fixtures, with the sample gauge length fixed by means of an adhesive exactly marking the length. The sample was initially placed with cellophane tape to lie exactly aligned along an annular piece of paper as shown in the schematic (Fig. 1). Once

as 20 MPa to as high as 350-400 MPa. Based on the tests the instantaneous strain, compliance and young's modulus was calculated. The fracture stress was plotted as a function of total strain (Fig. 6) as well as the Young's modulus (Fig. 7) to get an idea of the material behavior at room temperature. Both plots show an increasing trend. The scatter in these values is attributed to the inherent porosity in the foils that make it easy for crack propagation during tensile loading. The fracture surfaces reveal this clearly. Figs. 8 a is the fracture surfaces of the foil whose P Vs t plot is shown in Fig. 4, the crack can be seen to propagate from the pore. Also shown are the fracture surfaces of the same sample subject to a slightly higher strain rate of  $6 \times 10^{-4} \text{ s}^{-1}$  (Fig. 8b). Here again it can be seen that the failure occurs at a pore.

Based on these preliminary results, tests are being performed at high temperatures to check into the material behavior at these temperatures. Since porosity poses a big problem in the mechanical properties, compaction of these are also being tried out, to eliminate porosity and enable getting bulk materials.

#### **(B) The Al rich composition ( $\text{Al}_{90}\text{Cu}_7\text{Zr}_3$ )**

The microstructure here, although essentially made of the two eutectic phases, also contains the third phase (the metastable  $\text{Al}_3\text{Zr}$ ) in the as solidified foils (Fig. 9a and 9b). The latter occurs in pockets, as the primary phase on rapid quenching, followed by heterogeneous nucleation of Al, with the intermetallic  $\text{Al}_2\text{Cu}$  along the grain boundaries. The thermal stability studies of this alloy also shows a phase transformation at higher temperatures (Fig. 10 a-c). Room temperature testing of this alloy gave similar results to

that of the near eutectic composition with a scatter in the breaking loads and an increasing trend in the plots of the fracture stress as a function of total strain and Young's modulus.

### **The Al-Ni alloys**

The microstructural investigation of the rapidly solidified Al-(7-10)%Ni alloys with 1-3%Zr additions are carried out. The alloys containing 3%Zr yield a glassy matrix with a Al and  $Al_3Ni$  as the dispersed phase. The addition of 1%Zr yields very fine eutectic microstructure which on heat treatment yields nanometric dispersed microstructure. Cuboidal shaped  $Al_3Zr$  often nucleates the aluminium grains at the center resulting in a stable composite structure. The stability of this microstructure is studied in details. The results are discussed in details in the manuscript prepared for submission to a journal, which is enclosed in Annexure 1.4. The mechanical studies of these alloys has to be studied as a part of a future project.

# Annexure 1

- 1.1 Depression of melting point of multidomined bismuth in alumnium based metallic glass nanocomposites.  
R. Goswami and K. Chattopadhyay  
Appl. Phys. Lett. 69 (7) August 1996
- 1.2 Melting and superheating of metals and alloys  
K. Chattopadhyay and R. Goswami  
Progress in Materials Science (in press)
- 1.3 Nanocomposite microstructure in a melt spun Al-Cu-Zr alloy  
Dheepa Srinivasan and K. Chattopadhyay  
Materials Science Forum Vols. 243-245 (1997) PP. 251-256
- 1.4 Formation and coarsening of a nanodispersed microstructure in melt spun Al-Ni-Zr Alloy  
Dheepa Srinivasan and K. Chattopadhyay  
(To be submitted)

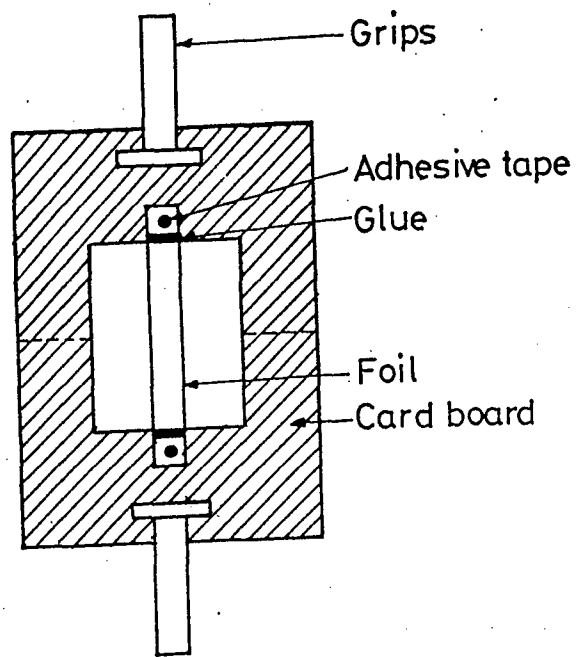


**Fig.1**

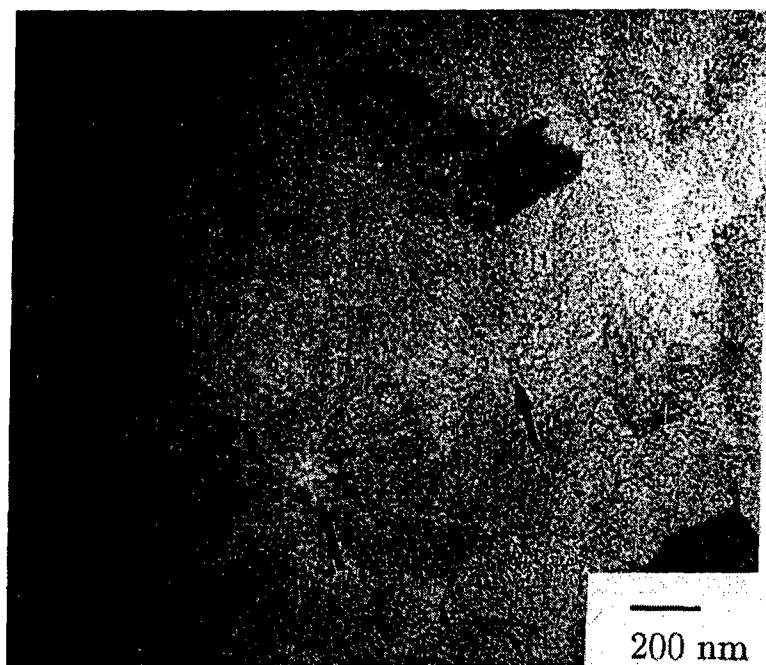


Fig.2a

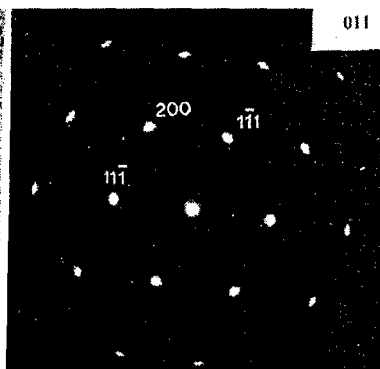


Fig.2b

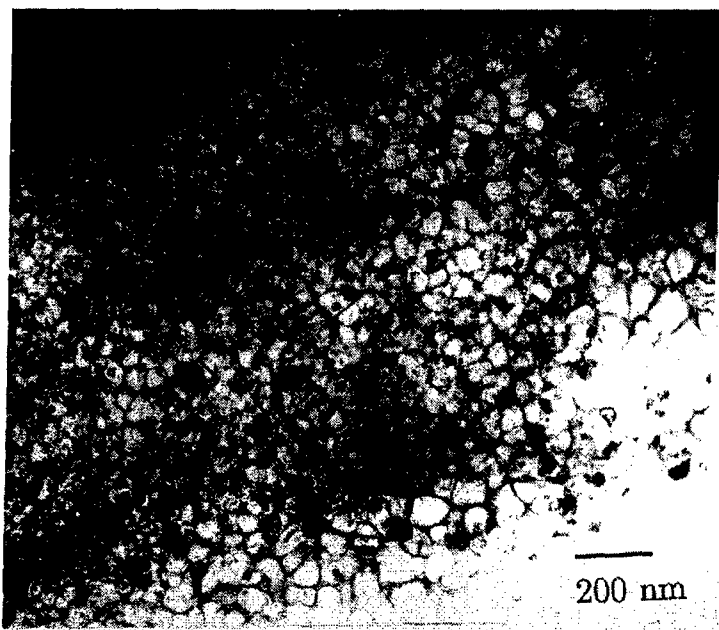


Fig.2c



Fig.2d

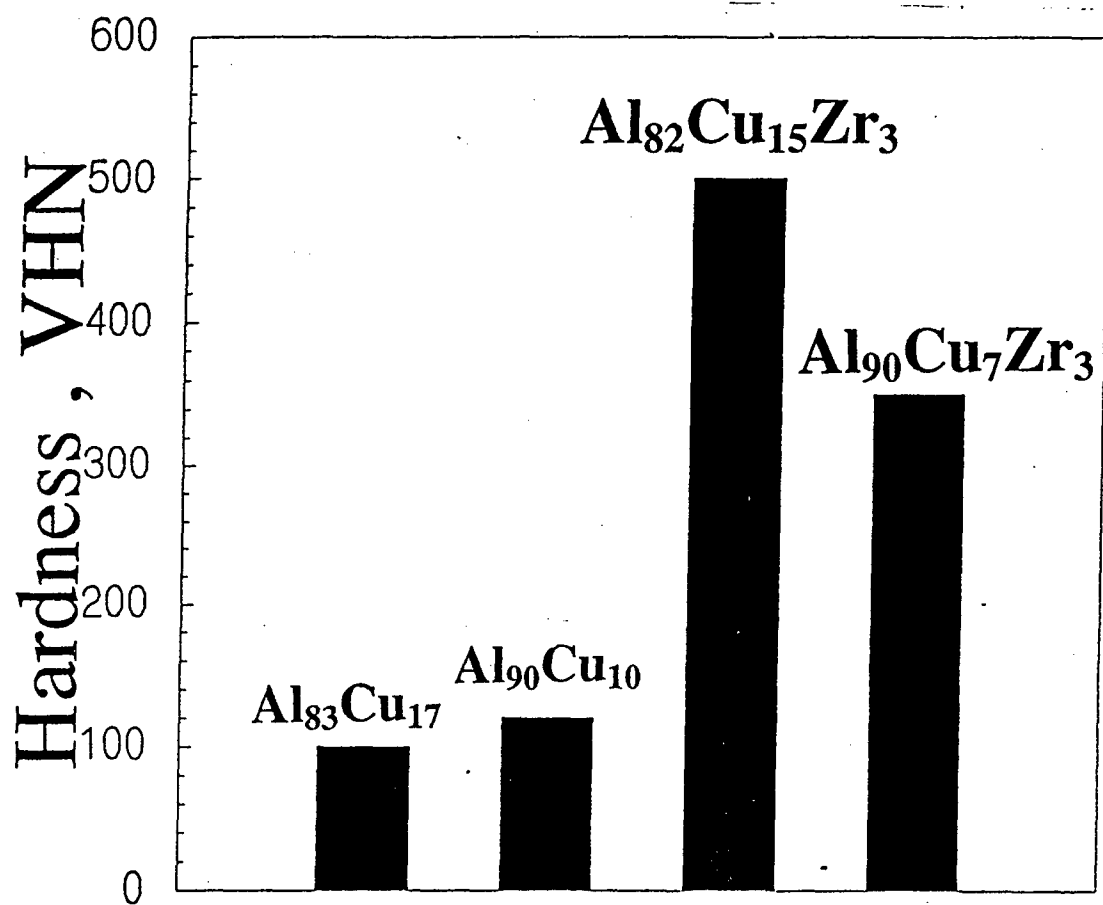


Fig.3

Table showing the scatter in the breaking load, compliance and Young's Modulus in the  $\text{Al}_{82}\text{Cu}_{15}\text{Zr}_3$  samples tested at room temperature

G L : 15 mm

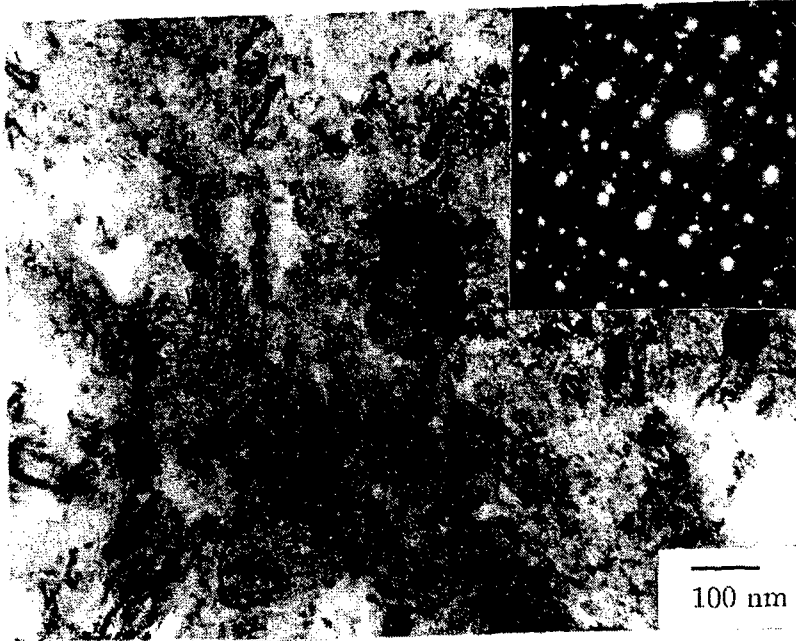
Cross head speed : 800 =  $\sim 3 \mu\text{m/s}$

1100 =  $\sim 6 \mu\text{m/s}$

Strain rates : 800 =  $2 \times 10^{-4} \text{ s}^{-1}$  (

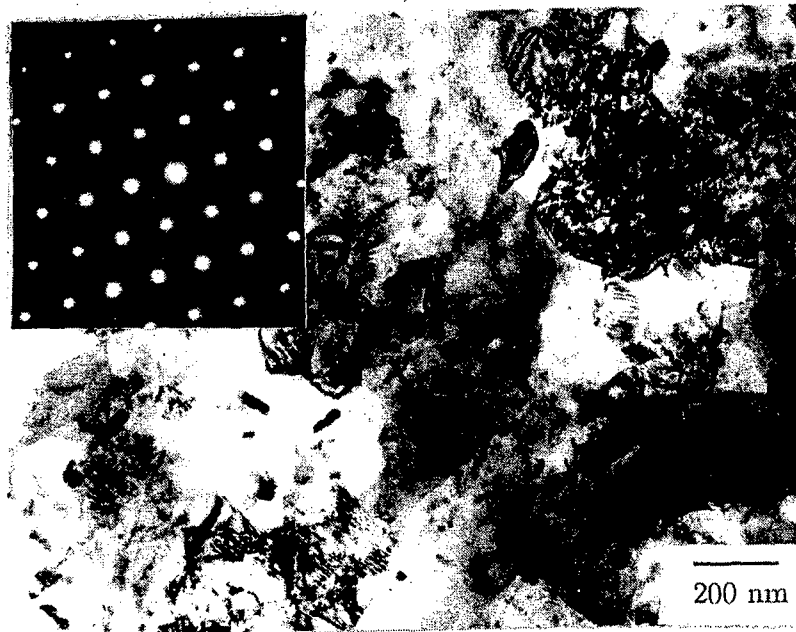
1100 =  $4 \times 10^{-4} \text{ s}^{-1}$

Sl. No	Sample Details	Thickness ( $\mu\text{m}$ ) / Width (mm)	Breaking Load (Kg)	Breaking Strength (MPa) / Total Strain (%)	Compliance $C_a$ ( $\text{mm N}^{-1}$ )	Y = L/CA (GPa)
1	T 35 (1100)	70 / 2.0	0.95	66.5 / 2.8		4
2	T 19 (800)	20 / 2.0	1.4375	352 / 6.8	0.0257	14
3	T 21 (800)	18 / 2.0	0.65	177 / 2.76	0.03540	11
4	T 20 (800)	20 / 2.0	0.60	147 / 2.1	0.0268	13
5	T 18 (800)	20 / 1.5	0.605	197 / 2.1	0.0265	18
6	T 41 (1100)	20 / 0.8	0.1833	112 / 1.2	0.0822	11
7	T 32 (1100)	15 / 1.0	0.142	92 / 1.0	0.09316	10
8	T 38 (1100)	10 / 1.0	0.105	103 / 0.68	0.0624	24
9	T 13 (800)	40 / 1.25	0.0925	18 / 0.8	0.1096	2.73
10	T 15 (800)	12 / 1.0	0.0875	70 / 0.21	0.0353	35
11	T 16 (800)	20 / 0.8	0.06	36 / 0.25	0.0720	13
12	T 31 (800)	20 / 1.0	0.039	19 / 0.54	0.09603	8
13	T 42 (1100)	20 / 1.0	0.0935	46 / 1.28	0.134	6



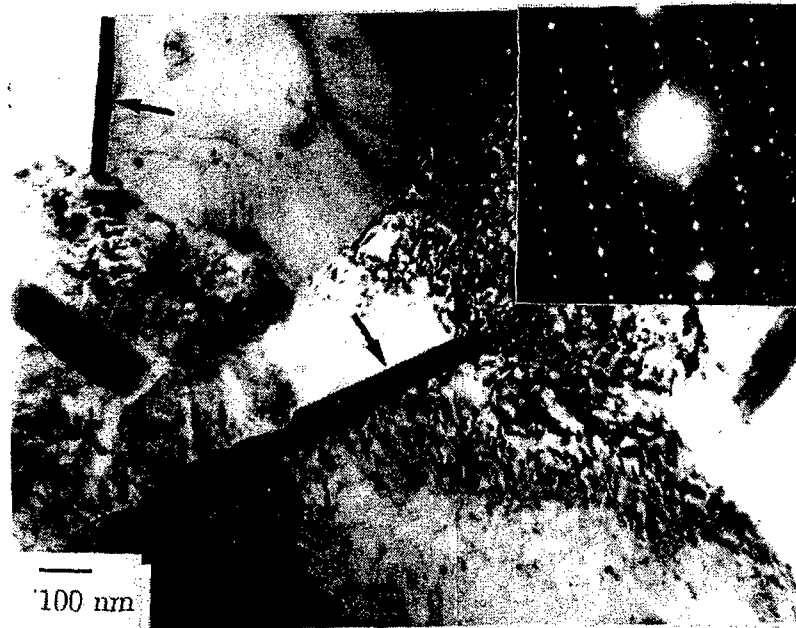
200 C, 1 h

Fig.4a



400 C, 1h

Fig.4b



500 C, 1h

Fig.4c

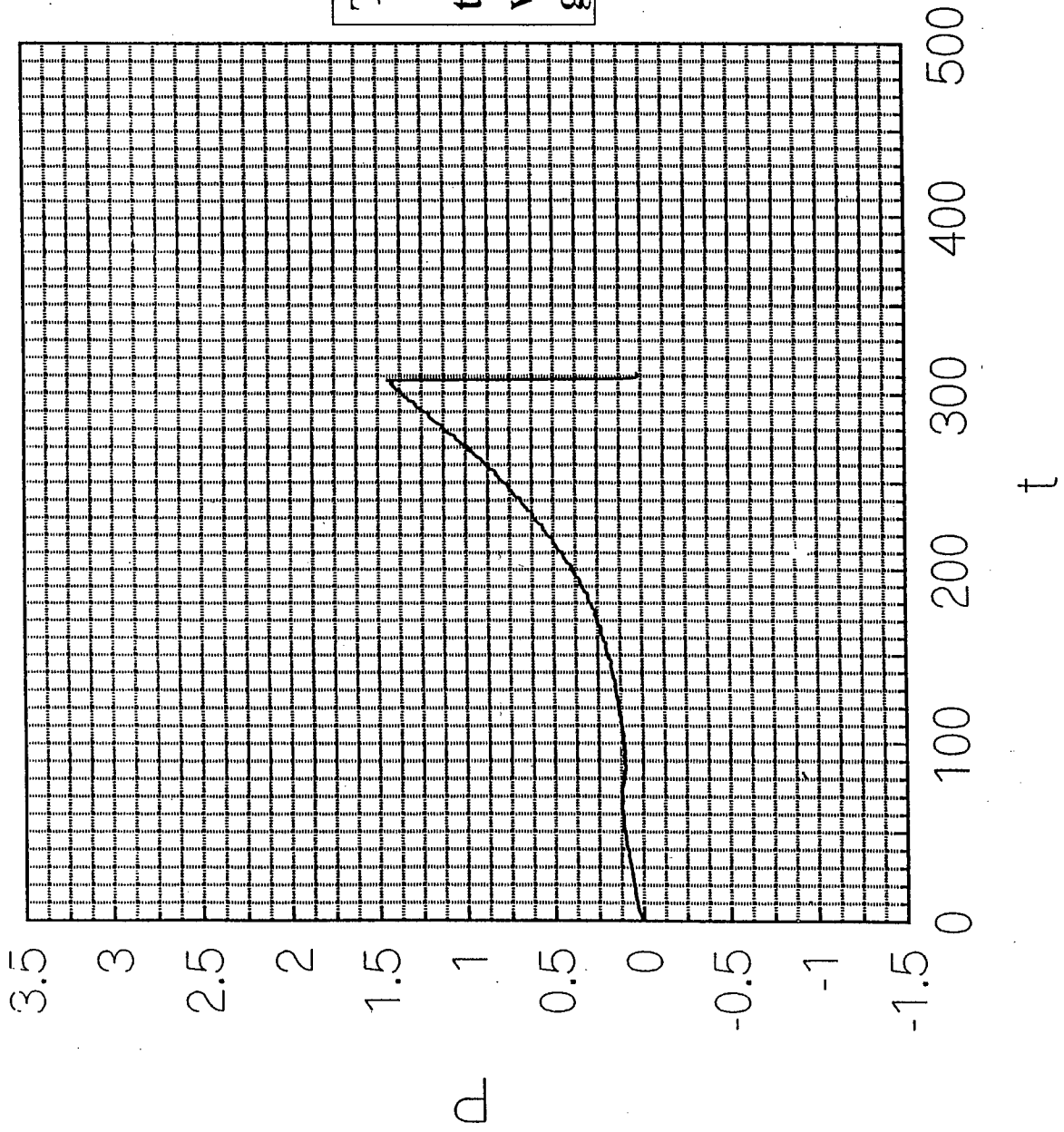


Fig.5

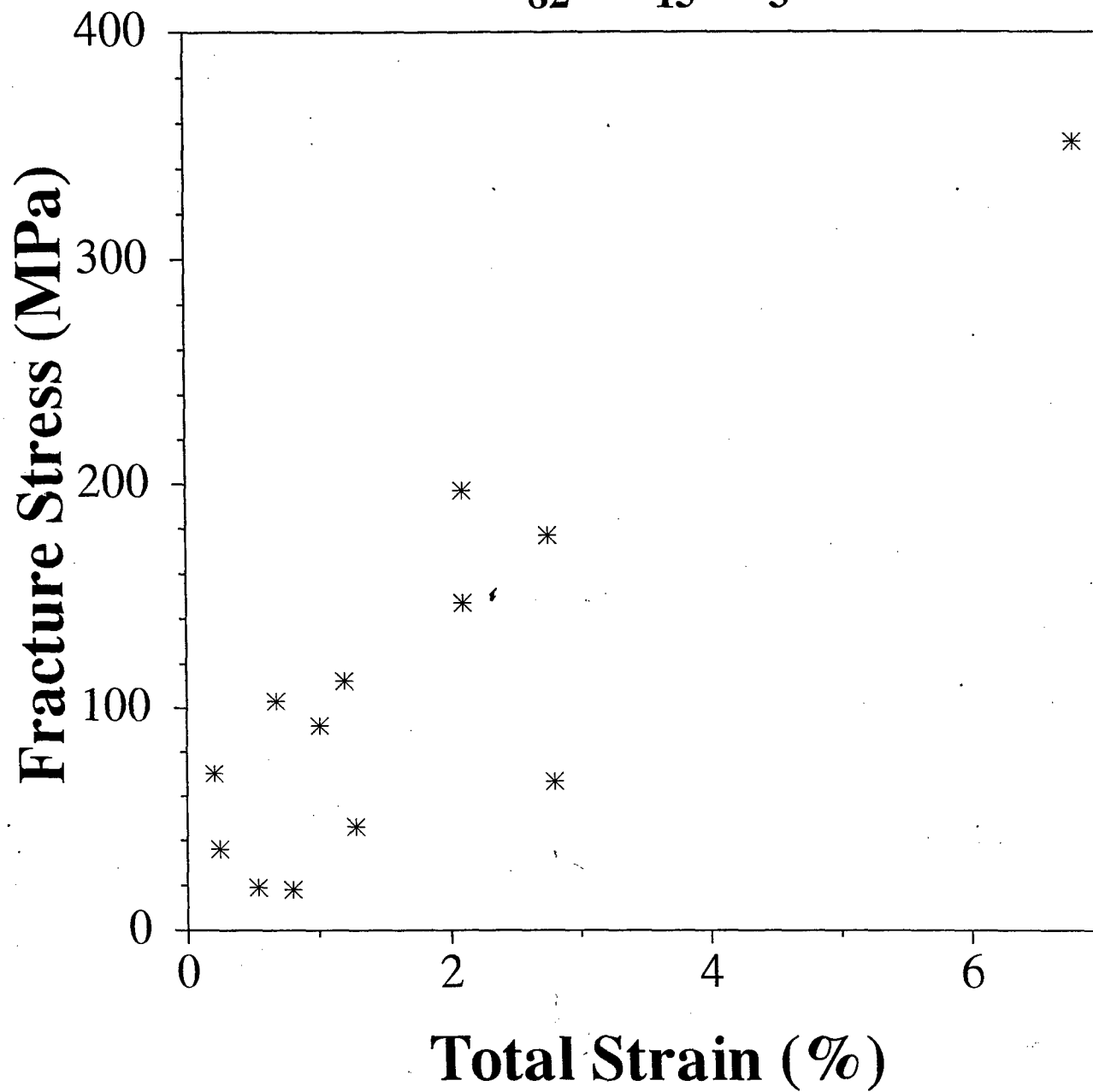


Fig.6

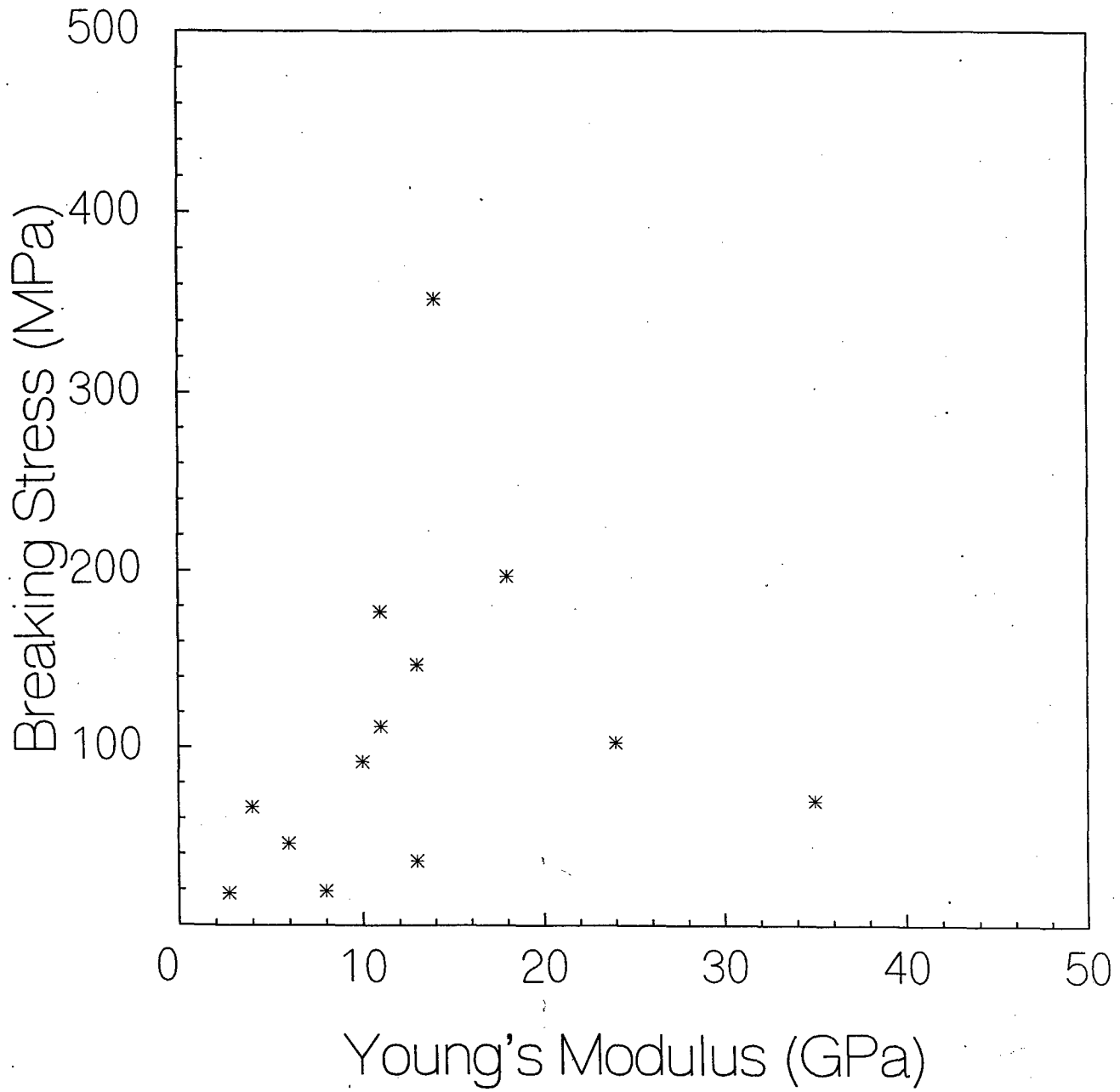


Fig.7

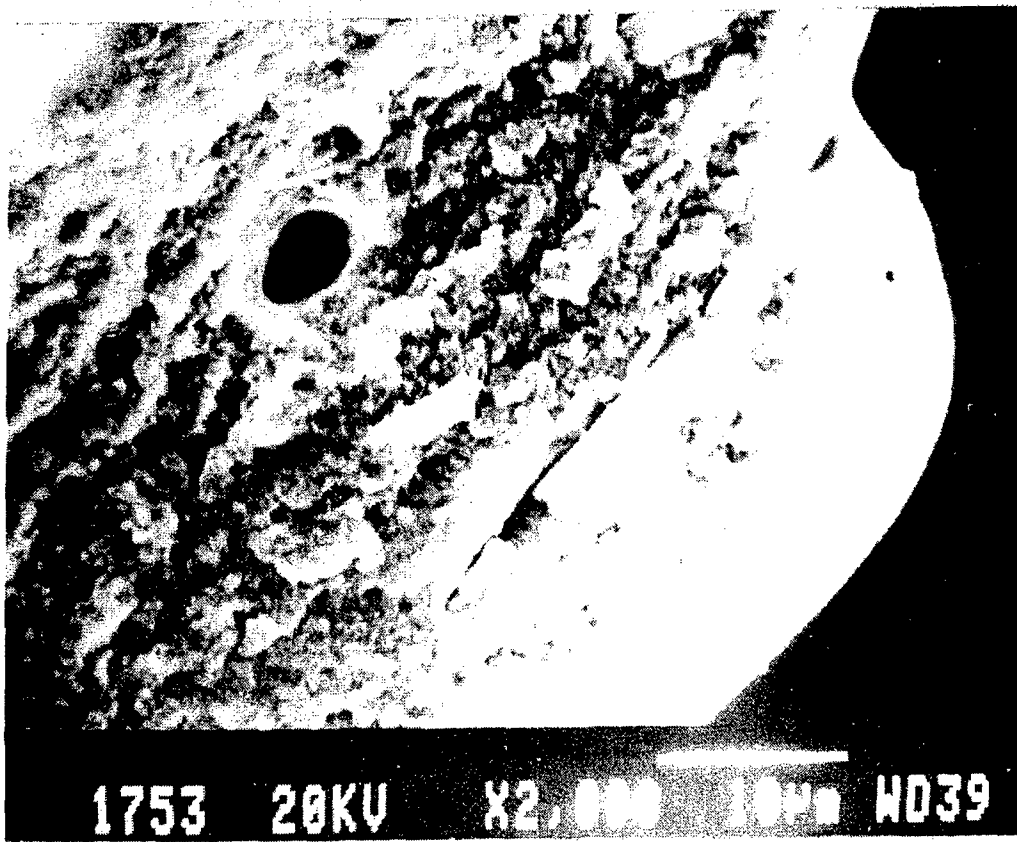
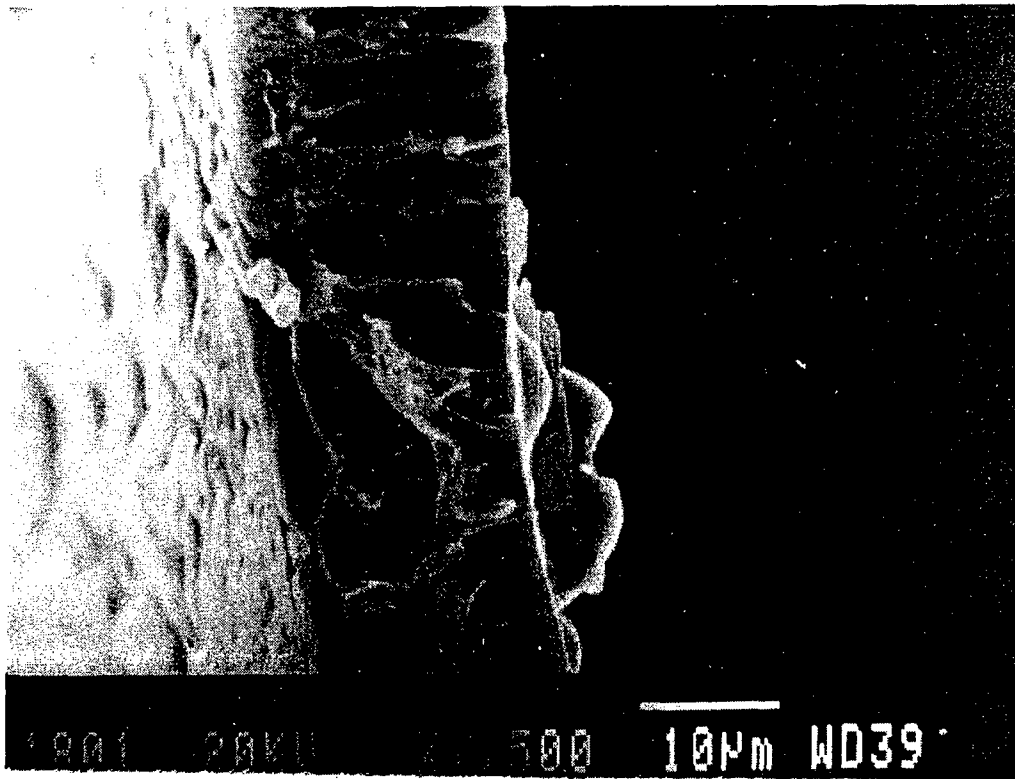
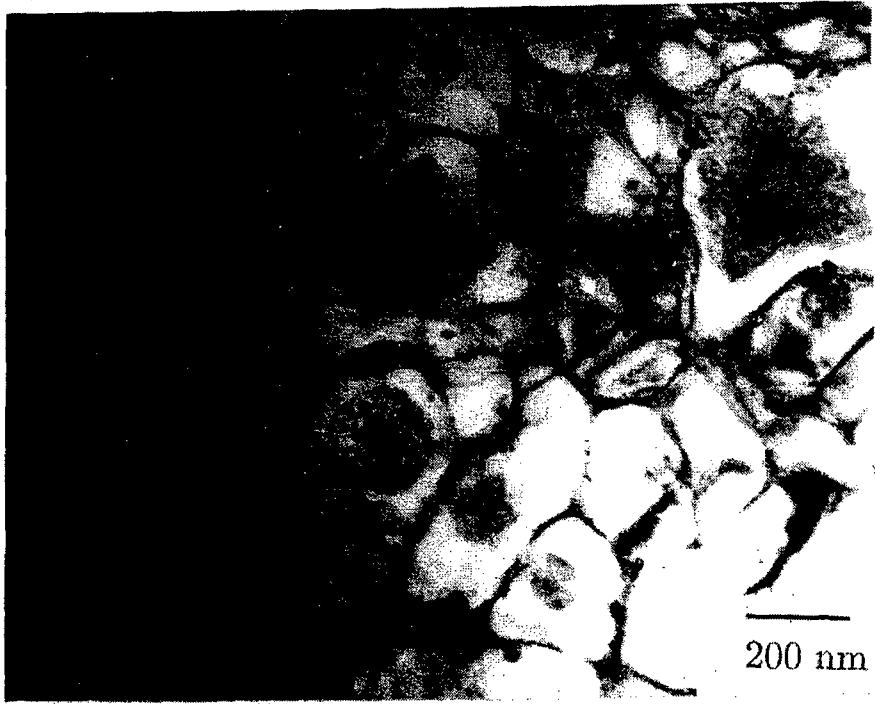
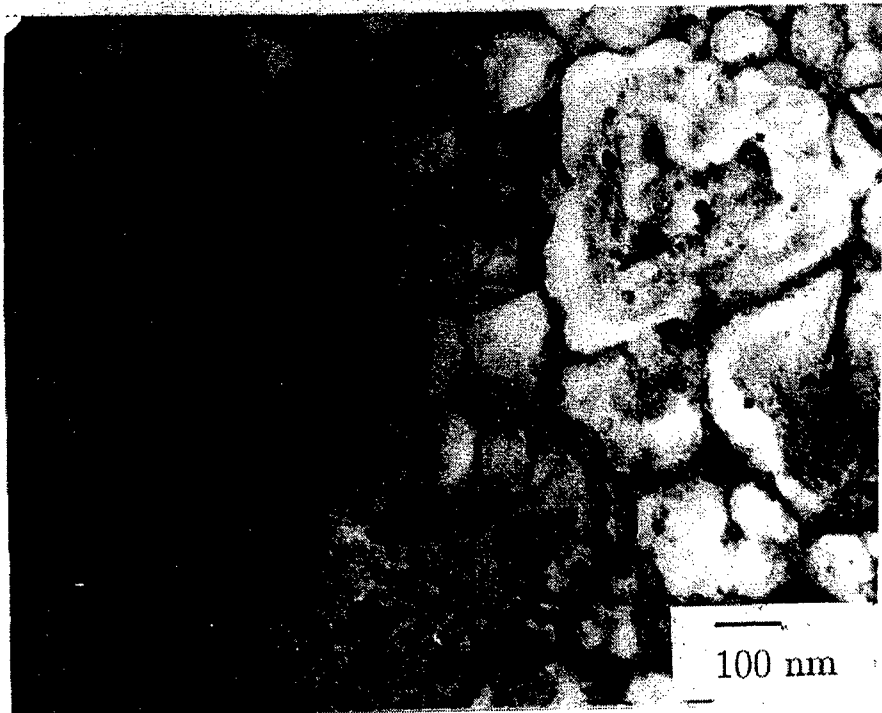


Fig.8



**Fig.9a**



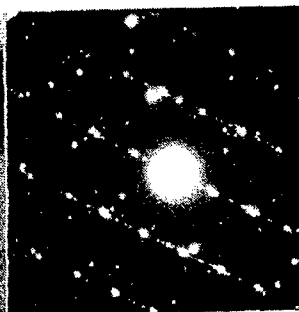
**Fig.9b**



200 C, 1h



400 C, 1h



500 C, 1h

Fig.10

(Received 15 September 1995; accepted for publication 31 May 1996)

We report the synthesis of nanocomposites of Bi in an aluminum based metallic glass matrix by rapid solidification. It is shown that constrained melting and solidification of nanometer sized embedded Bi particles lead to the formation of symmetry related multidomained particles. The Bi particles exhibit a significantly large depression of bulk melting point (over 100 K) requiring a free energy gain of greater than  $0.7 \times 10^8 \text{ J m}^{-3}$ . This cannot be explained by the size dependence of melting points or other pressure effects and represents an intrinsic characteristic of the multidomained particles. © 1996 American Institute of Physics. [S0003-6951(96)00733-4]

Controlling the nucleation of the phase separating liquid prior to the solidification, using the rapid solidification processing techniques, can provide a promising route to manufacture a class of nanocomposites where nanoscaled particles are embedded in a crystalline matrix.<sup>1,2</sup> Such a material can have wide application in nanotechnology including antifriction materials. A suitable addition of alloying elements offer the possibility of avoiding the solidification of the matrix and thereby, producing a composite of nanocrystalline particles embedded in a metallic glass matrix. In this letter we report synthesis of nanosized Bi particles in an aluminum based glassy matrix and show that the constraining influence of the glassy matrix leads to multiple domain formation in the initial single-crystal particles during cycling through melting and solidification. Following this, we report and discuss an unusual depression of the bulk melting point of these embedded Bi particles.

Al and Si are miscible in molten state and form an eutectic system with very little solubility in the solid state at room temperature.<sup>3</sup> The addition of the Fe stabilizes the melt and promotes the formation of the metallic glass.<sup>4</sup> The interactions of Bi with all these three elements are highly repulsive and are reflected in the appearance of liquid immiscibility in binary couples.<sup>3,5</sup> The phase diagrams also indicate that the solid solubility of Bi with the three elements are negligible in solid state. Thus, interaction of Bi with Al-Si-Fe is also expected to yield liquid immiscibility and should provide opportunity for synthesizing nanometric dispersion of Bi in glassy Al-Fe-Si matrix. We have chosen a known glass forming composition  $\text{Al}_{65}\text{Si}_{15}\text{Fe}_{20}$  for our study.

The alloys are prepared from high purity (>99.999%) constituent elements by induction melting and rapidly solidified using melt spinning technique. The analyzed composition in atom percent is  $\text{Al}_{65}\text{Si}_{16.4}\text{Fe}_{19.4}\text{Bi}_{0.7}$ . The ribbon samples were characterized by a JEOL FXII transmission electron microscope (TEM) and thermal studies were carried out under dynamic argon atmosphere using a Perkin Elmer DSC IIC differential scanning calorimeter (DSC) with a heating and cooling rate of 20 K/min.

A typical microstructure of the nanocomposite is shown

in Fig. 1(a). The electron diffraction pattern [Fig. 1(b)] confirms the existence of glassy matrix and crystalline rhombohedral Bi. The sizes of the Bi particles vary between 5–30 nm with a log normal distribution. The glassy matrix is stable up to 585 K. The decomposition process is complete at 700 K. Electron diffraction of the quenched samples from above this temperature indicates a crystalline matrix having a tetragonal crystal structure ( $a=0.612 \text{ nm}$  and  $c=0.943 \text{ nm}$ ).

Most of the Bi particles in as solidified state was found to be single crystal. However, cycling the samples above the melting point of Bi (but below the crystallization point of the glass) and subsequent cooling leads to a major change in the morphology of the Bi nanoparticles. Most of the particles (>80%) after third cycle show crystallographically distinct multiple domains (Fig. 2).

The results of the investigation on melting and solidification behavior of the nanometric Bi can be summarized as follows. The Bi melts with an onset at 523 K and a peak at 545 K in the as-cast condition. In the rapidly solidified samples, a small fraction of the Bi particles starts melting fairly early and over a range of temperature. These do not give any resolvable endothermic peak. However, stopping the heating cycle and cooling from a lower temperature [460 K for Fig. 3(a)] yield a distinct and sharp solidification peak indicating the occurrence of melting. In addition, one observes a broad endothermic peak with an onset at 503 K and

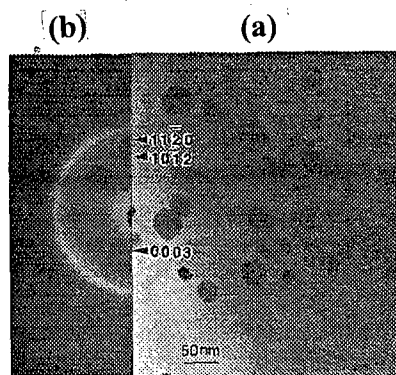


FIG. 1. (a) A bright field micrograph showing the distribution of the nanometric Bi particles in metallic glass matrix in a rapidly solidified sample of  $\text{Al}_{63.5}\text{Si}_{16.4}\text{Fe}_{19.4}\text{Bi}_{0.7}$  alloy. (b) Selected area diffraction pattern from the above showing the diffuse ring due to metallic glass and the sharper rings due to Bi particles.

<sup>a)</sup>Electronic mail: kamanio@metallrg.iisc.ernet.in

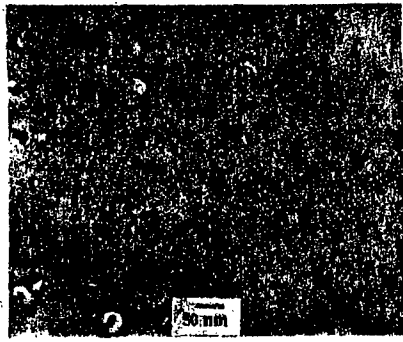


FIG. 2. A bright field micrograph showing multiple domained particles of Bi after heating the sample to 560 K and cooling to room temperature. Note the difference in contrast due to multiple domains in a single particle.

serves a broad endothermic peak with an onset at 503 K and a peak at 523 K [Fig. 3(b)] corresponding to the melting of the majority of the particles. Beyond the third cycle, the DSC curve consistently shows a broad melting peak at 442 K [Fig. 3(c)] with an occasional peak at 389 K [Fig. 3(d)]. No other melting peak could be observed. Considering the as-cast peak of 545 K, the observed melting point of 442 K represents a depression of 103 K. We also note that, although the majority of the particles melted near this temperature, the breadth of the peak and the occasional observation of the small peak at 389 K indicate the existence of a spectrum in the depressed melting of nanoparticles of Bi (~50 K). In contrast, the solidification always occurs with a relatively sharper peak at 367 K for all the cases (Fig. 3). A quantitative evaluation of the solidification exotherm of the Bi particles melted just after the peak at 442 K and after the sample heated up to 570 K indicates that 80% of the Bi particles have already been melted at the end of the depressed melting peak. *In situ* melting experiments inside the electron micro-

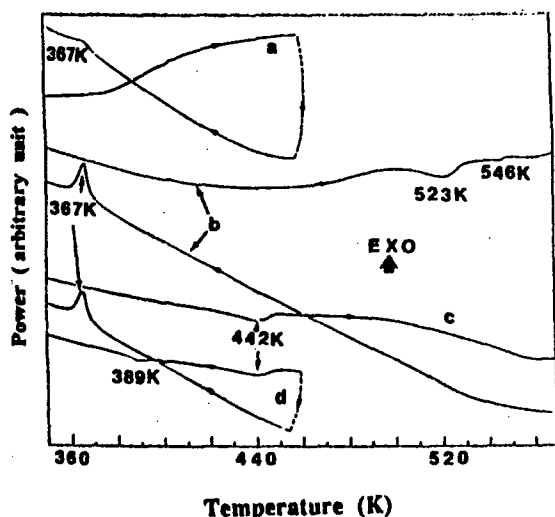


FIG. 3. DSC thermograms revealing the melting and solidification behavior of the nanometric Bi particles. (a) Thermogram of as-spun sample cycled up to a temperature of 460 K. (b) Same as above but cycled up to 580 K. (c) Thermogram of the third cycle of a sample. In each cycle the sample is heated up to 580 K and cooled to room temperature. Note the depressed melting of the sample. (d) DSC trace of the same sample as "c". The cycle is interrupted after the depressed melting peak and cooled.

scope using the dark field technique of imaging confirmed the melting point depression of Bi particles. However, these experiments suggest that the depression shown by the particles are statistical in nature and the same particle often shows different behavior in different cycles.

The formation of the multiple domained nanometric particles during constrained solidification is a new observation which requires an explanation. Multiply twinned particles were observed earlier in nanoparticles obtained by the condensation of vapor.<sup>6</sup> We argue that the occurrence of crystallographic variants is related to the requirement of preserving the symmetry of the initial liquid cavity without the loss of continuity at the interface. Considering the diffusion distance,<sup>7</sup> the shape of the nanosized liquid cavity can be approximated to the equilibrium shape, primarily due to the very short equilibration time that is needed. Therefore, the number of variants needed during solidification for preserving the cavity shape is given by the order of the intersection group of the matrix and the dispersoid.<sup>8</sup> For the glassy matrix it is infinity. The actual number, however, will be dictated by the heterogeneous nucleation kinetics in the constrained liquid which will promote these variants. It is clear that the number increases during recycling and this aspect needs further study.

In order to understand the observation on melting we have calculated the free-energy difference ( $\Delta G$ ) between the liquid and solid at the depressed melting temperature from the knowledge of the specific heat of undercooled melt<sup>9</sup> and using the expression  $\Delta G = \Delta S_0 \Delta T - \int \Delta C_p dt - T \int (\Delta C_p / T) dt$ . The entropy of freezing  $\Delta S_0$  for Bi is  $0.93 \times 10^6 \text{ J m}^{-3}$ . The energy difference needed for the depression of the melting point from the equilibrium value to the temperature range of 389–440 K is estimated to be  $0.7 \times 10^8 - 0.9 \times 10^8 \text{ J m}^{-3}$ . The Bi particle expands when it solidifies. This generates a compressive pressure over the Bi particles. The volume free energy due to this strain is estimated to be  $0.05 \times 10^8 \text{ J m}^{-3}$ .<sup>10</sup> This is negligible compared to the energy required for the melting at 442 K.

In order to rationalize the melting behavior, a number of effects have been considered. The size effect has been calculated using the model of Buffat and Borel.<sup>11</sup> It is observed that the size of the free particle should be below 2 nm to expect a depression of melting observed in the present experiments. The minimum size of the particle experimentally observed is 5 nm. In a free state this will yield a melting point of 490 K. The effect of the constraining surfaces in the embedded case is to increase the melting point in comparison to the free state and the magnitude depends upon the contact angle of the nucleating liquid.<sup>12,13</sup> Thus the size effect cannot explain the observed behavior.

In an alloy, the reduction of size can also lead to enhanced solubility. However, since Bi has repulsive interactions with all the matrix atoms (Al, Fe, and Si), the surface energy difference for glassy and crystalline matrices will not be very different. We are successful in crystallizing the matrix by rapid heating without a significant change in the size of the dispersed Bi particles. The DSC melting experiments using these samples do not exhibit any depression of Bi melting point. In case the solubility is responsible for melt-

very high undercooled level ( $\Delta T=220$  K) a metastable form of Bi has been observed.<sup>15</sup> In the present case, careful diffraction studies using the x-ray and electron as well as high resolution electron microscopy did not reveal any metastable phase in any samples including the ones which showed depression of melting of 80% of particles. Our experimental observation thus rules out the possibility of the origin of the depressed melting peak due to the presence of metastable Bi.

Fecht has already proposed a model for the defect mediated depression of melting point.<sup>16</sup> Attempts to explain the presently observed depression of melting point in terms of vacancies and dislocations have yielded an unrealistically high defect concentration. Analysis of our various results clearly suggest that the appearance of the domain boundaries play an important role in the melting point depression. However the exact mechanism and quantitative confirmation is required in the future to understand the observed phenomenon.

To conclude, we have reported the formation of nanocomposites of Bi particles in a metallic glass matrix and have shown that under a constrained solidification condition, they yield particles with multiple domains. We also report an un-

The work is supported by grants from DAE and DST, Government of India. Additional support came from AOARD under Contract No. F49620-95-1-0105.

- <sup>1</sup>R. Goswami and K. Chattopadhyay Acta Metall. Mater. 42, 383 (1994).
- <sup>2</sup>R. Nagrajan and K. Chattopadhyay, Acta Metall. Mater. 42, 947 (1994).
- <sup>3</sup>Binary Alloy Phase Diagram, edited by T. B. Massalski (ASM, Metals Park, OH 1982).
- <sup>4</sup>A. Inoue, M. Yamamoto, H. M. Kimura, and T. Masumoto, J. Mater. Sci. Lett. 6, 194 (1987).
- <sup>5</sup>A. K. Nissen, F. R. deBoer, R. Boom, P. F. de Chatel, W. C. M. Matson, and A. R. Miedema, CALPHAD 7, 51 (1983).
- <sup>6</sup>S. Ino, J. Phys. Soc. Jpn. 27, 941 (1969).
- <sup>7</sup>W. P. Eljjs and N. H. Nachtrieb, J. Appl. Phys. 21, 804 (1950).
- <sup>8</sup>J. W. Cahn and G. Kalonji, in Solid-Solid Phase Transformation, edited by H. I. Aaronson, D. E. Laughlin, R. F. Sekerka, and C. M. Wayman (TMS, Warrendale, 1983), p. 3.
- <sup>9</sup>I. H. Perepezko and S. J. Pulk, J. Non Cryst. Solids 61, 111 (1994).
- <sup>10</sup>D. R. Uhlman, J. Non Cryst. Solids 41, 347 (1980).
- <sup>11</sup>Ph. Buffat and J.-P. Borel, Phys. Rev. A 13, 2287 (1976).
- <sup>12</sup>R. Goswami and K. Chattopadhyay, Philos. Mag. Lett. 68, 215 (1993).
- <sup>13</sup>H. Saka, Y. Nishikawa, and T. Imura, Philos. Mag. A 57, 895 (1988).
- <sup>14</sup>C. J. Holman, J. Phys. Chem. Solids 36, 1249 (1975).
- <sup>15</sup>J. H. Perepezko, in Second International Conference on Rapid Solidification Processing: Principle and Processing, edited by R. Mehrabian, B. H. Kear, and M. Cohen (Claitor's, Baton Rouge, 1980), p. 56.
- <sup>16</sup>H. Fecht, Nature 356, 133 (1992).



# MELTING AND SUPERHEATING OF METALS AND ALLOYS

*K. Chattopadhyay\*\* and R. Goswami†*

\*Department of Metallurgy, Indian Institute of Science, Bangalore, 560 012, India and †Institut Fuer Werkstoffphysik und Structureforschung, University of Bremen, Post Fach 330440, D-28334, Bremen, Germany

## CONTENTS

1. INTRODUCTION	000
2. SOLIDIFICATION AND MELTING AS PROBLEMS IN CLASSICAL NUCLEATION	000
3. MELTING VIEWED AS AN INSTABILITY IN THE SOLID	000
4. THE CRYSTALLOGRAPHIC SHAPE AND THE MELTING OF SMALL PARTICLES	000
5. THE MELTING OF EMBEDDED PB PARTICLES: THE CASE OF SUPERHEATING	000
6. THE DEPRESSION OF MELTING POINT OF EMBEDDED PARTICLES: THE CASE OF BI	000
7. CONCLUDING REMARKS	000
REFERENCES	000

## 1. INTRODUCTION

Through a series of articles in Nature, <sup>(1-4)</sup> Professor R.W. Cahn has repeatedly brought to focus the progress achieved and the problems to be solved in the basic but fascinating field of melting of solids. At a personal level, he has constantly encouraged us to work in this field. It is, therefore, a great honor to write this article in an issue dedicated to Professor Cahn. We shall concentrate on the melting of small particles and in particular, embedded small particles which have been studied less extensively. The issue which is of primary interest to the materials community in this research area and the subject matter of the present article is the observed asymmetry in the solidification and melting behavior of metals and alloys.

## 2. SOLIDIFICATION AND MELTING AS PROBLEMS IN CLASSICAL NUCLEATION

Let us consider the case of liquid to solid transformation involving a single solid phase. The transformation is characterized by the symmetry breaking of the infinite symmetry of the liquid to the allowed point group symmetry of the crystalline solid. The free energies of the solid and liquid phase will intersect at the temperature corresponding to thermodynamic melting or freezing point of the phase. However, experiments have shown that solidification in general initiates at a temperature lower than the thermodynamic freezing temperature. In contrast, melting normally initiates at or just above this

\*Author for correspondence.

temperature (Fig. 1). The classical theory of nucleation <sup>(5,6)</sup> in most cases successfully explains the observed undercooling during solidification. According to this, the additional energy of the interface associated with the appearance of a new phase acts as a barrier to the kinetic process of nucleation. The same theory in principle can be extended for the

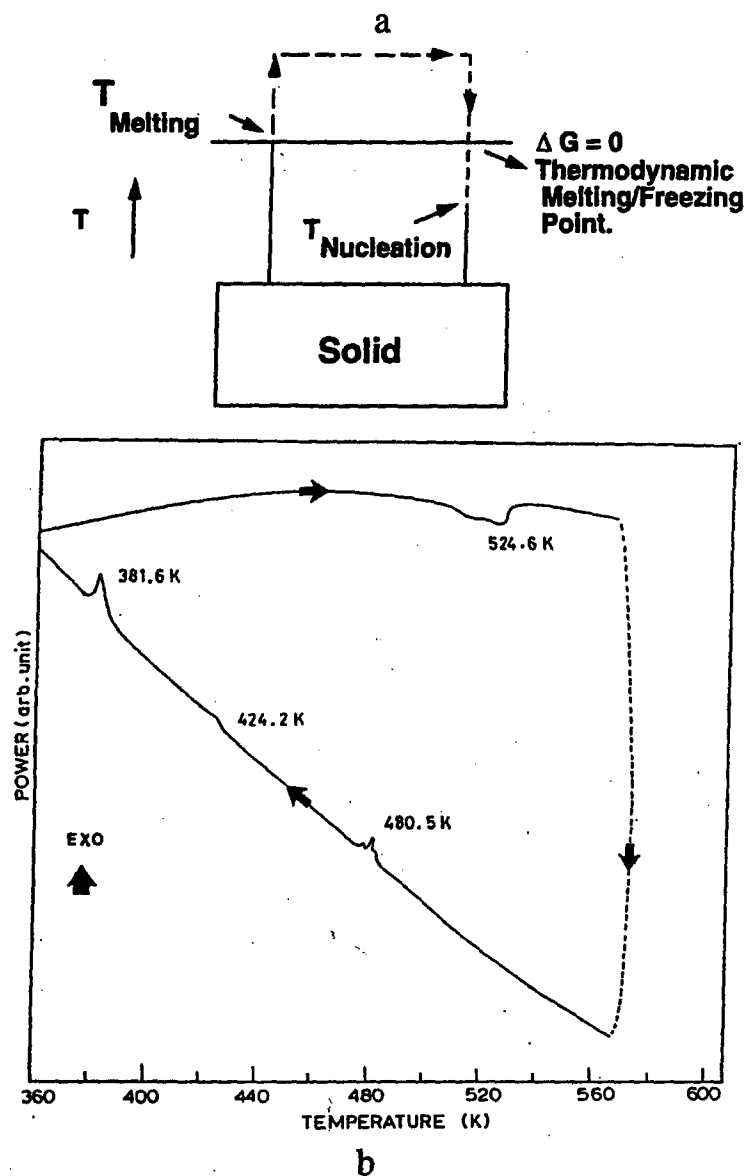


Fig. 1. (a) A schematic diagram highlighting the asymmetry in melting and solidification of a solid. (b) A typical DSC curve for the melting and solidification of embedded Bi particles highlighting the asymmetry of the melting and solidification. The multiple solidification peaks below the thermodynamic melting point indicate heterogenous nucleation of Bi from its melt by different catalytic sites. No such spread and superheating could be observed for the case of melting.

melting case. The balance of surface energies at the interface ensures that the sites favorable for the nucleation of solid will be unfavorable for the nucleation of melt. Therefore, the system showing low undercooling during solidification is expected to show superheating. Extension of the classical theory of nucleation to the case of melting has been discussed by Uhlmann.<sup>(7)</sup> He has also incorporated the strain effect due to volume change which reduces the effective driving force and thus increases the superheating. To date no experimental report is available for the homogenous nucleation of the melt inside the solid. Therefore, extension of the homogenous nucleation theory to melting is of academic interest and lack practical importance. Heterogeneous nucleation of the melt, on the otherhand, is distinctly possible since all the experimental evidences suggest the initiation of melting at the solid-vapor surfaces and at the internal boundaries of the solid.

### 3. MELTING VIEWED AS AN INSTABILITY IN THE SOLID

The majority of the theoretical works on melting attempt to explain the melting phenomenon in terms of an instability. Lindemann<sup>(8)</sup> first proposed a criterion for melting which continues to attract serious attention. This can be stated as follows. Melting is a vibrational instability released when the root mean square amplitude of vibration reaches a critical fraction (10%) of the interatomic distance. Several investigators attempted to calculate the critical temperature for different planes when this instability will appear.<sup>(9-11)</sup> However, it is only recently that conclusive experimental evidence of the relationships among crystallography, the Debye temperature and the melting temperature of various surface planes has been obtained. These data were gathered for a single crystal of lead.<sup>(12, 13)</sup> Attempts have been made to establish the upper bound of the superheated state.<sup>(14, 15)</sup> As pointed out by Fecht and Johnson,<sup>(14)</sup> there exists an equivalent critical point for melting similar to the Kauzman temperature (the ideal glass transition temperature) in the case of solidification. The latter is defined as the temperature where the entropy of the solid is equal to that of the liquid. Below this temperature, the solid will have higher entropy and an entropic instability will occur in the crystalline phase leading to the formation of glass. Similar entropic instability will also exit at higher temperature for superheated solid leading to the formation of liquid. As pointed out by Tallon,<sup>(16)</sup> this will be the uppermost instability point and there may exist several other instabilities for superheated solid including the shear instability proposed by Born<sup>(17)</sup> and the volume instability by Tallon et al.<sup>(18)</sup> which can lead to the formation of liquid.

The only one of these the instabilities for which there is any experimental evidences is that of Lindemann. The experimental evidence of surface melting of different crystallographic planes at different temperatures below the thermodynamic melting point and the increase of the melted layer thickness as the temperature approaches the thermodynamic melting point<sup>(12, 13)</sup> clearly supports this criterion. However experiments also indicate that certain planes do not melt at or below the thermodynamic melting temperature contrary to this criterion.<sup>(31, 32, 39)</sup> We shall come back to this issue in a later section. Historically, most of the melting experiments have dealt with small size samples for two reasons. The first is the same as that for performance of nucleation experiments in solidification on small particles, namely, the higher probability that the nucleation in some of the particles will be free of the relevant impurity effect. The size effect also provides additional insights into the melting process.

#### 4. THE CRYSTALLOGRAPHIC SHAPE AND THE MELTING OF SMALL PARTICLES

A large number of investigations on the melting of small particles of low melting point elements such as lead, indium, tin and bismuth have been reported in the literature. <sup>(19-25)</sup> The onset of melting of these particles is found to take place significantly below the bulk melting point. The results indicate an inverse relation of melting point depression with particle size. Several theoretical models <sup>(26-29)</sup> have been proposed to explain this depression; those have been recently reviewed. <sup>(29)</sup> The current results strongly suggest the presence of a surface melted layer <sup>(13,14)</sup> which plays important role in the initiation of the melting process.

Contrary to the size dependence of melting point, relatively little effort has been devoted to understand the influence of crystallographic shape on the melting point. Allen et al. <sup>(30)</sup> have shown that the plate shaped particles do not show any size dependent depression of melting point. At least two experimental results on entrained Bi and Pb exist which suggest that the superheating ability may be related to shape. <sup>(31,32)</sup> Spiller, <sup>(31)</sup> in particular, has presented clear evidence of a superheating of 2 K above the bulk melting point of Pb for large triangular platelets. The result of Metois and Heyraud <sup>(32)</sup> that triangular shaped particles of lead bounded by {111} planes show a 3 K superheat essentially reconfirms this experimental result. One problem in these experiments is the lack of temperature calibration. The melting of the surrounding irregular particles is normally regarded as the bulk melting temperature. The possibility of the depression of melting of these particles cannot be ruled out.

There is a growing interest in recent time on the melting behavior of the embedded particles. The effect of embedding was first discussed by Allen et al. <sup>(25,30)</sup> The clear evidence of superheating due to embedding was first observed for Ag crystals embedded in Au matrix by Dages et al. <sup>(33)</sup> During the same period large superheating of embedded solid Ar in Al matrix has been reported. <sup>(34)</sup> Following this, several investigations have dealt with the melting behavior of the embedded particles. <sup>(38, 39, 42, 44-47, 57)</sup> In the rest of this article, we shall present the current results on the melting behavior of the embedded particles of Pb and Bi primarily focusing on some of our recent work in the field.

Fortunately both Pb and Bi forms immiscible system with a large number of elements having higher melting points. Monotectic points lie near the high temperature end of these systems. Rapid solidification of alloys close to the monotectic composition yields a nanometric dispersion of the low melting phase in the high melting matrix. The origin of this microstructure is discussed elsewhere. <sup>(35, 40, 56)</sup> One of the distinctive feature of the microstructure of these nanodispersed materials is the observation of orientation relations with the matrix. Clearly the liquid dispersion of the low melting element solidifies through heterogeneous nucleation catalyzed by the surrounding matrix. We have studied four different matrices having close packed structures (Al, Cu, Ni and Zn) with Pb as the nanodispersed phase. For Bi, we have chosen Zn and Al as the crystalline matrices. In addition we have studied the effect of metallic glassy matrix by selecting a glass of Al-Fe-Si. All the components of the glass exhibit a repulsive interaction with Bi. <sup>(55)</sup>

Table 1. Table showing the orientation relations, intersection group and the shape of embedded Pb and Bi particles in various closed packed matrices

System	Orientation Relation	Matrix Point Group	Intersection Group	Shape
Zn-Pb hcp-fcc	$(0001)_{Zn} \parallel (111)_{Pb}$ $[11\bar{2}0]_{Zn} \parallel [1\bar{1}0]_{Pb}$	6/mmm	$\bar{3}m$	Truncated hexagonal biprism
Zn-Bi hcp-rhomb	$(0001)_{Zn} \parallel (01\bar{1}2)_{Bi}$ $[11\bar{2}0]_{Zn} \parallel [2110]_{Bi}$	6/mmm	$\bar{1}$	Truncated hexagonal bipyramid
Cu-Pb fcc-fcc	$(111)_{Cu} \parallel (111)_{Pb}$ $[1\bar{1}0]_{Cu} \parallel [1\bar{1}0]_{Pb}$	m3m	m3m	Truncated cuboctahedron
Al-Pb fcc-fcc	$(111)_{Al} \parallel (111)_{Pb}$ $[1\bar{1}0]_{Al} \parallel [1\bar{1}0]_{Pb}$	m3m	m3m	Truncated cuboctahedron
Ni-Pb fcc-fcc	$(100)_{Ni} \parallel (100)_{Pb}$ $[011]_{Al} \parallel [001]_{Pb}$	m3m	4/mmm	Truncated cuboctahedron

## 5. THE MELTING OF EMBEDDED PB PARTICLES: THE CASE OF SUPERHEATING

A summary of the orientation relationships between Pb particles and the different matrices is given in Table 1. A cube-cube orientation relationship is observed in the case of both Al and Cu matrices in spite of large difference in the lattice parameters for the two cases (for Al  $a_0 = 0.4049$  nm and for Cu  $a_0 = 0.3614$  nm). The Zn matrix yields a Burgers orientation relation while Ni shows a different orientation relation. In most cases the particles exhibit distinctive shapes. The observed point group symmetries of the particle shapes are also included in the Table 1. These can be compared with the point group symmetry of the equilibrium shapes of the embedding particles. These are obtained from the intersection group. For the case of the liquid inclusion, the shape will be given by the matrix point group while for the case of the embedded solid, the intersection group of the two solids at the observed orientation relation is needed for determining the point group of the equilibrium shapes. These are also included Table 1. Careful transmission electron microscopy permits us to determine the shapes. Typical projected shapes of the embedded lead particles in Al and Zn matrices are listed in Table 1 and illustrated in Fig. 2.

The melting of the embedded particles was studied by differential scanning calorimetry. <sup>(38)</sup> The advantages of this technique are high sensitivity and accurate temperature measurements which yield reliable data for comparison. However, the information can be correlated only indirectly with the microstructure. Table 2 gives a summary of the observed melting points. The table also gives the minimum and maximum particle size observed in these samples. A few points deserve specific mention. Although there exists a spread in the particle size, the DSC melting peaks do not reflect this spread. For the case of Cu and Ni matrices, the undercooling for solidification is negligible. Further, though Pb embedded in a Cu matrix exhibits significant superheating, the onset of melting for Pb in the Ni matrix in melt spun alloys is lower than the onset of the solidification. Superheating of Pb was also not observed in the melt spun Zn-Pb alloys. These results can be compared with the results of Peppiat <sup>(36)</sup> for free crystals of Pb and the results of Cheyssac et al. <sup>(37)</sup> where the Pb particles were embedded in alumina. For the purpose of comparison, we have presented in Table 3 the observed melting point in each case corresponding to the minimum size in our embedding experiments. In both these cases, the lead particles exhibit a depression of melting point. Our recent experiments on Pb embedded in glassy silica matrix also do not show any superheating.

Although for the cube-cube orientation relation the point group symmetry of the

equilibrium shape remains unaltered for solid and liquid lead, it is not true for other orientation relations. In order to probe the influence of shape on melting, Zn-Pb melt spun samples were heat treated for 30 hours at 550 K. The heat treatment shows a definite

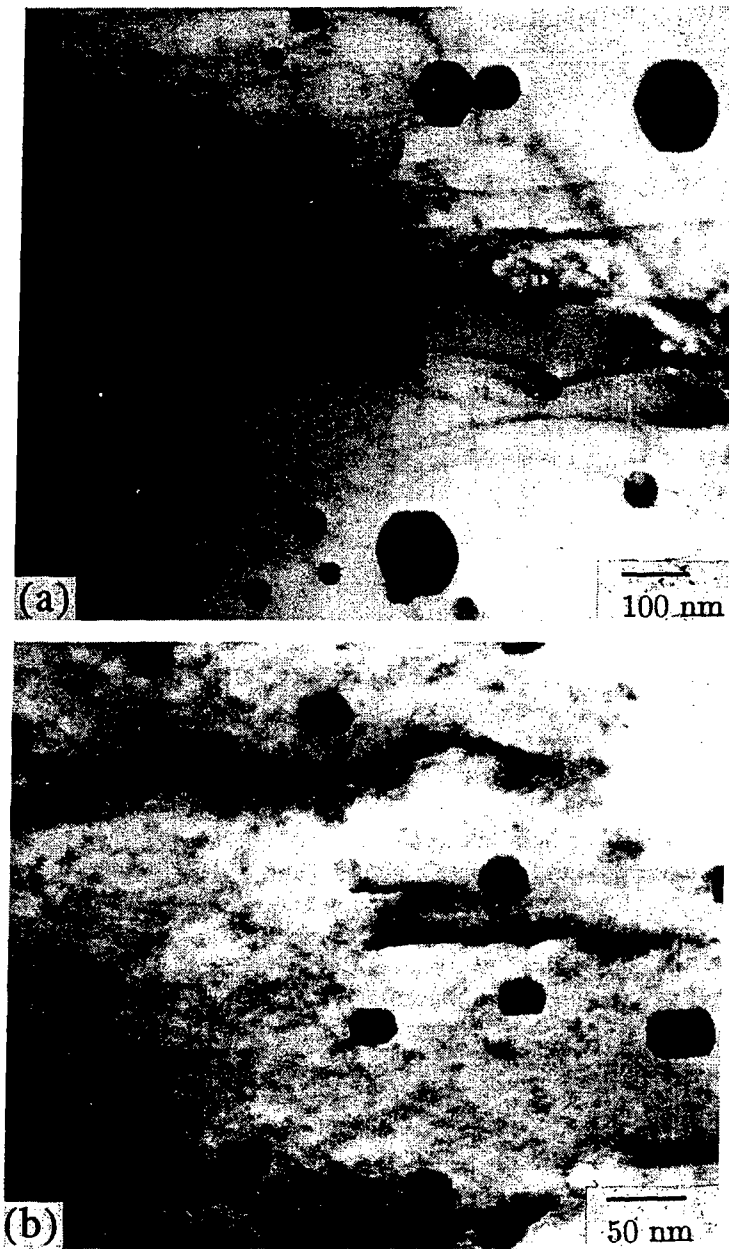


Fig. 2. Transmission electron micrograph of the projected shape of Pb particles embedded in Al and Zn matrices. (a) For the case of Al matrix viewed along [110] of Al. (b) The case of Zn matrix viewed along [1120] of the matrix.

Table 2. The observed particle size, melting and the solidification peaks of embedded Pb particles in melt spun alloys. The transformation temperatures are determined from the differential scanning calorimeter experiments

	Particle Size (nm)		Equilibrium melting point K	First MeltingK	Superheating Peak K	Solidification Peak K
	Min.	Max.				
Al-Pb	10	70	599.8	597	703	568
Cu-Pb	25	210	599	593	724	598
Ni-Pb	30	120	600	595	-	591
Zn-Pb	4	130	591	579	-	549.5

change in shape (Fig. 3). Significantly some of the Pb particles after the heat treatment exhibit distinct superheating of 62 K. <sup>(39)</sup>

Since embedded particles are constrained, it is necessary to evaluate various pressure effects on the melting point of the particles for a comparison with the experimental results. There exists three pressure effects. These are 1) the capillarity effect due to decreasing size, 2) differential thermal expansion between the matrix and the particle and 3) effect due to volume change during melting. Couchman and Jesser <sup>(27)</sup> have developed equations for the size dependent change in melting point. For the embedded case they find:

$$T_{ml}/T_0 = 1 - 3(\sigma_{sm}/\rho_s - \sigma_{lm}/\rho_l)/(rL_0) \quad (1)$$

Here  $T_{ml}$  is the melting point of the embedded particle and  $T_0$  is the bulk melting point.  $\sigma_{sm}$  and  $\sigma_{lm}$  are the solid particle/matrix and liquid/matrix interfacial energy,  $L_0$  is the latent heat per unit mass and  $\rho_s$  and  $\rho_l$  are the densities of solid and liquid.

The pressure effect due to differential thermal expansion of the matrix and the embedded phase has been considered by Spaepen and Turnbull. <sup>(41)</sup> The pressure difference is given by

$$\Delta P = [12(\alpha_p - \alpha_m) \cdot \Delta T \mu_m k_p] / (3k_p + 4\mu_m) \quad (2)$$

Here  $\alpha_p$  and  $\alpha_m$  are the linear thermal expansion coefficient and  $k_p$  and  $\mu_m$  are bulk modulus of the precipitate and shear modulus of the matrix. The effective change in melting point can be obtained from the Clausius Clapeyron equation:

$$\Delta T = \Delta P T_0 \Delta V / L_r \quad (3)$$

The effect of change in volume during constrained solidification has been discussed by Uhlmann <sup>(7)</sup> and recently by Malhotra and Aken. <sup>(42)</sup> The volume change leads to an additional strain energy which results in a reduction in the driving force for solidification. The change in free energy due to strain is given by <sup>(7)</sup>

Table 3. A comparison of melting points of Pb observed in present investigation and those reported by other investigators

Size (nm)	Present work	Observed change in Melting Point ( $T_{obs} - T_{eq}$ )K	
		Kofman et al.[29] (embedded in $Al_2O_3$ )	Peppiatt & Sables[23] (Free Particles)
10 (Al-Pb)	103	- 90	< - - 40
25 (Cu-Pb)	125	- 40	- 30
30 (Ni-Pb)	- 5	- 40	- 20 to - 30

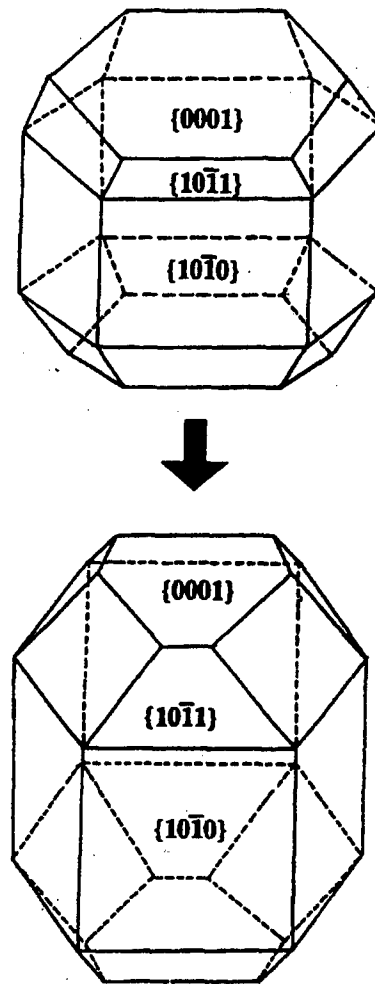


Fig. 3. A schematic diagram illustrating the observed shape change in the nano sized Pb particles embedded in Zn matrix in a melt spun alloy before and after an equilibration heat treatment.

$$\Delta G_{st} = (2\mu_s k_l \Delta V^2) / (3k_l + 4\mu_s) \quad (4)$$

where  $\mu_s$  is the shear modulus of the entrained solid,  $k_l$  is the bulk modulus of the entrained liquid and  $\Delta V$  is the relative volume change. This reduction in driving force has to be compensated by superheating. There exist several models for correlating the free energy change in the undercooled melt<sup>(43)</sup> which can be extended to superheated solids. For example, Graebeck and Bohr<sup>(46)</sup> have adopted the Hoffman's model<sup>(48)</sup> and expressed the free energy change as

$$\Delta G_r = L_v \Delta T (T/T_0^2) \quad (5)$$

where  $L_v$  is the enthalpy of fusion per unit volume and  $T_0$  is the equilibrium melting point. The condition  $\Delta G_v = \Delta G_{st}$  gives the superheating needed due to the volume strain.

All these pressure effects for the case of lead embedded in Al, Cu, Ni and Zn matrices

are given in Table 4 together with the maximum observed superheating peak. Clearly the explanation of the observed results on the basis of the pressure effect is unsatisfactory for nanosized embedded particles. A similar conclusion was arrived at by Cantor and co-workers<sup>(57,60)</sup> who suggested the relief of pressure at the interface due to the vacancy and creep cavitation. The qualification of nanosize is necessary since there exists recent work on the melting behavior of the micron sized particles of in Al matrix which is adequately explained by pressure effect owing to the volume strain energy during melting.<sup>(42)</sup>

The above discussions point to the need for understanding the kinetics of melting and the role the interface may play in the case of embedded particles. Application of the classical nucleation theory is possible for the case of melting of a solid. However, in this case one has to account for the strain effect due to volume change for estimating the driving force for the nucleation. Incorporating this it was found that the superheating requirement for a detectable nucleation rate ( $1 \times 10^{23} \text{ m}^{-3} \text{ s}^{-1}$  for the present case computed by considering the sensitivity of the DSC used) is  $\sim 160 \text{ K}$ . This upper kinetic limit is generally much lower than the limit posed by entropic instability and has greater practical significance. This is because, unlike the cases of solidification and glass formation, the diffusivity and hence the atomic jumps causing homogenous fluctuation do not diminish with increasing superheating. This means that spontaneous melting by homogenous nucleation probably cannot be bypassed unless the heating rate is extremely high. The experimental results, however, indicate that a much lower superheating is achieved, suggesting the possible role of heterogeneously nucleated melting. Since the geometry of the bounding interfaces is well known in the nanometric case, we first consider the stability of the liquid phase (Pb) at the interface between the solid Pb and the matrix.

In the case of the fcc matrix of Al and Cu, the bounding planes are  $\{111\}$  and  $\{110\}$  of both Pb and the matrix phase. Introduction of a liquid layer at the interface results in the replacement of the solid–solid interface by the two liquid–solid interfaces facing the matrix and the particle respectively. Thus the stability of the liquid layer will be controlled by the changes in surface energy  $\Delta\gamma$ . The condition for stability for the  $\{111\}$  interface is given by

$$\Delta\gamma = \gamma_{m111-Pb111} - \gamma_{m111-Pb1} - \gamma_{Pb111-Pb1} > 0 \quad (6)$$

Here  $\gamma_{m111-Pb111}$  is the interface energy between the  $\{111\}$  planes of the matrix and the solid Pb,  $\gamma_{m111-Pb1}$  is the interface energy of the liquid Pb and the matrix  $\{111\}$  planes and  $\gamma_{Pb111-Pb1}$  is the interface energy of the liquid Pb and  $\{111\}$  planes of the solid Pb. Although the absolute values of liquid–solid interface energies are difficult to estimate, the data on

Table 4. Table showing the influence of different pressure effects on the change in melting point of lead in Kelvin. The positive sign indicate an increase in melting point. The fourth column indicate the cumulative effect and the numbers in the last column indicate the effective superheating/depression of melting point corresponding to observed values for the melt spun alloys when the presue effects are taken into consideration

	Volume	Thermal	Size	Total $\Delta T$ (calc.)	$\Delta T$ (expt.)
Al-Pb	17	4	54 (10)	75	103
Cu-Pb	17	14	48 (25)	79	125
Ni-Pb	17	26	53 (30)	96	- 45
Zn-Pb	17	- 47	40 (10)	10	( - 7)
		+ 20		77	

heterogeneous nucleation kinetics during solidification enable obtaining the interface energy difference between the solid–solid and solid–liquid interfaces to be evaluated. For example, Moore et al. <sup>(49)</sup> have estimated the difference in matrix–liquid Pb and matrix–solid Pb surface energies as  $51 \text{ mJ m}^{-2}$  on  $\{111\}$ . Al facets. Strictly the interfacial energies obtained from the nucleation experiments are valid for the temperature of the onset of solidification. In the case of Pb nucleating on Al, it is around 575 K. For the case of melting, the surface energy difference must be evaluated at the observed melting temperature. It is experimentally shown, however, that the effect of entropy is not significant for the Al–Pb solid–solid interface. <sup>(49)</sup> This behavior is probably characteristic of an immiscible system. Hence the equation 6 implies that the temperature dependence of the surface energy of the liquid Pb–Al interface will mainly influence the stability of the interface. The surface energy of any general surface can be expressed as

$$\gamma = u - TS \quad (7)$$

where  $u$  is the excess surface internal energy and  $S$  is the excess surface entropy. The internal energy can have a chemical origin from the bond breaking and forming at the interface and for an immiscible system it is expected to scale with the excess heat of mixing. Additionally one can have a structural component. The last term in the equation 7 controls the temperature dependence of the interfacial energy. Thus this will basically determine the critical temperature where  $\Delta\gamma$  will be zero for a given system and the extremum condition for liquid to be stable at the matrix–particle solid–solid interface. For low value of excess surface entropy, the superheating is expected to be high.

Although the above reasoning is specific to  $\{111\}$  type of interfaces, it can also be extended to  $\{100\}$  interfaces. From the knowledge of the equilibrium shape and the temperature dependence of interfacial energy anisotropy which can be experimentally obtained <sup>(49)</sup> it is shown that the liquid Pb is not stable with respect to  $\{100\}$  solid–solid interface at the melting point. <sup>(38)</sup> Thus a superheating is to be expected. This rationalizes the observations in Table 2 for the melting of Pb in Al and Cu matrices since the particles are bounded by  $\{111\}$  and  $\{100\}$  type of interfaces.

A quantitative estimate of superheating from the consideration of the mechanical stability of the liquid at the interface requires knowledge of the entropy term. The importance of this term can be judged from our result on Pb particles in a Zn matrix. <sup>(39)</sup> The observation of superheating only after an equilibration heat treatment (which does not alter the bounding planes) points to the crucial role of interfacial defects. Clearly these symmetry related defects have profound influence on the excess surface entropy and hence on the superheating ability.

#### 6. THE DEPRESSION OF MELTING POINT OF EMBEDDED PARTICLES: THE CASE OF BI

In the case of Pb embedded in Ni an effective depression of melting point could be observed. The depression was also observed for some of the Pb particles in copper matrix by Kim and Cantor <sup>(50)</sup> and Cd particles in Al matrix. <sup>(57–59)</sup> Our results on Ni corroborate these observations although we additionally observe a small superheating peak. These investigators attribute the depression of melting point to size effect. For the embedded cases, this implies that the average matrix–liquid interface energy is higher than the average matrix–liquid surface energy. <sup>(39,57)</sup> We note that, in such a case, the depression represents

Table 5. Table showing the melting points in degree K of Bi under different conditions

	Zn-Bi	Glassy Al-Fe-Si + Bi
Equilibrium Alloy	527.5	527.5
Melt Spun	520-535 (broad)	523
Melt Spun + > two cycles	434	442, 389
Depression of Melting Point	93.5	85.5, 138.5

constrained equilibrium. The results of solidification of the embedded particles of Pb in the Cu matrix indicate undercooling of less than a degree below the freezing point.<sup>(50)</sup> This is above the temperature of constrained equilibrium and therefore, difficult to explain by a kinetic reasoning. Thus the depression of melting point of the embedded particles pose major difficulty in our understanding. However, the most dramatic results of the depression of melting point could be observed in the case of Bi particles in various matrices. This will now be presented.

As shown by Peppiat,<sup>(36)</sup> the free particles of Bi exhibit a size dependent depression of melting point. For the embedded case, the melting point can be shown to increase due to size effect.<sup>(27,44)</sup> Two of our recent experiments<sup>(51,52)</sup> are of particular significance in this regard. The melting behaviors of Bi embedded in a crystalline Zn and glassy Al-Fe-Si obtained by rapid solidification have been studied with differential scanning calorimetry. The details of the synthesis are given elsewhere.<sup>(40)</sup> The Bi particles in as-melt spun samples melt close to the equilibrium melting point though a few degrees of superheating could be observed in some of the samples. Solidification of the embedding melt occurs with an undercooling of 145.5 K for Zn and 160.5 K for a metallic glassy matrix. Cycling the samples through melting and solidification yields a surprising result. A small fraction of the Bi particles melt with a large depression of melting point. The reversible nature of this depressed melting point was established by stopping the experiments after the appearance of the depressed melting peak and cycling through solidification. The solidification behavior was found to remain unchanged and the depressed melting peak reappeared. Table 5 summarizes the results for the case of Zn and glassy matrices. In both cases, the pressure effects cannot explain the observations. One obvious explanation is the formation of the metastable Bi phases. However, both x-ray diffraction and the high resolution electron microscopy rule out any change in the crystal structure. The electron microscopy of the recycled samples revealed multiple crystals in each droplet (Fig. 4). This can be contrasted with the single crystal observed in each droplet in the melt spun samples. The Pb particles in a Ni matrix which show a depression of the melting point also consist of multiple crystal. The satisfactory explanation of this depression of the melting point is currently not available. However, there may be a link between this and the depression of the melting point in nanoscaled polycrystalline materials.<sup>(53)</sup> A recent comparative study of nanodispersed Al-Pb alloys obtained by rapid solidification and mechanical alloying is significant.<sup>(54)</sup> While in the former case, superheating of Pb particles can be observed, the mechanically alloyed samples show a depression of the melting point.

## 7. CONCLUDING REMARKS

Our recent experimental results summarized in the preceding sections highlight the importance of the crystallographic shape in the melting transition. It is clear from the

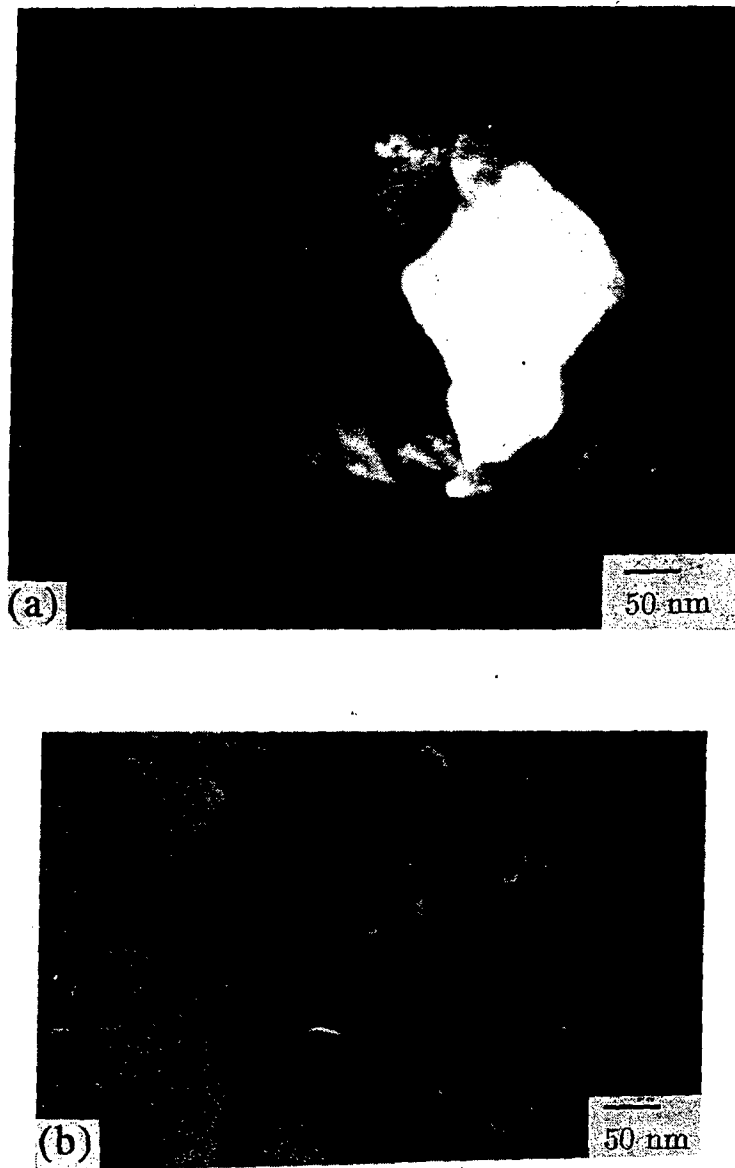


Fig. 4. The figure illustrate the multidomained particles which are generally associated with the depression of melting point of the embedded particles.a) A dark field micrograph of a Pb particle embedded in Ni matrix showing the crystallographic domains. Such particles show a depression of melting point of 5 K.b) A bright field microstructure of Bi particles embedded in a glassy matrix of Al-Fe-Si alloy obtained by melt spinning. The observed multidomained microstructure in each embedded particle appears only after thermal cycling of the sample through melting and solidification for more than two times. Simultaneously a large depression of melting points could be observed.

evidence to date that the interface plays an important role in the melting transition of embedded nanoparticles. While observation of the superheating is expected, the depression of the melting point in the embedded case is unusual. Even for the case of superheating, quantitative estimates which matches with the observed superheating are lacking. In order to gain further understanding, it will be necessary to probe the roles of chemical and crystallographic factors including the defect state at the interfaces. Only then, will it be possible to understand the temperature dependence of the interface energy and entropy which is a prerequisite to quantitative understanding of melting. Future work also needs to address the sites of and the mechanism for the initiation of melting at solid-solid interfaces.

#### ACKNOWLEDGEMENTS

The author take this opportunity to thank Professor S. Ranganathan, Professor B. Cantor, Professor P. Ramachandrarao and Mr. N. Ravishankar for many stimulating discussions. Financial support from the Board of Nuclear Research, Department of Science and Technology, Government of India and US Airforce Office of Scientific Research are gratefully acknowledged

#### REFERENCES

1. R. W. Cahn, *Nature* **273**, 491 (1978).
2. R. W. Cahn, *Nature* **323**, 668 (1986).
3. R. W. Cahn, *Nature* **334**, 17 (1988).
4. R. W. Cahn, *Nature* **342**, 630 (1989).
5. Christian, J. W. (1975) *Theory of Transformation in Metals and Alloys*, Pergamon, London.
6. D. Turnbull, *J. Appl. Phys.* **21**, 1022 (1950).
7. D. R. Uhlmann, *J. non-crystalline Solids* **41**, 347 (1980).
8. F. A. Lindemann, *Phys. Z.* **11**, 609 (1910).
9. B. Chatterjee, *Nature* **275**, 203 (1978).
10. L. Pietronero and E. Tosatti, *Solid State Communication* **32**, 255 (1979).
11. C. S. Jayanth, E. Tosatti and L. Pietronero, *Phys. Rev.* **B31**, 3456 (1985).
12. B. Pluis, A. W. Denier van der Gon, J. W. M. Frenken and J. F. van der Veen, *Phys. Rev. Lett.* **59**, 2678 (1987).
13. J. W. M. Frenken, P. M. J. Maree and J. F. Van der Ween, *Phys. Rev.* **B34**, 7506 (1986).
14. H. J. Fecht and W. L. Johnson, *Nature* **334**, 50 (1988).
15. S. Lele, P. Ramachandrarao and K. S. Dubey, *Nature* **336**, 567 (1988).
16. J. L. Tallon, *Nature* **342**, 658 (1989).
17. M. Born, *J. Chem. Phys.* **7**, 591 (1939).
18. J. L. Tallon, W. H. Robinson and S. I. Smedley, *Nature* **266**, 337 (1977).
19. M. Takagi, *J. Phys. Soc. Japan* **9**, 359 (1954).
20. J. Pocza, A. Barna and P. Barna, *J. Vac. Sci. Technol.* **6**, 472 (1969).
21. M. Stowel, T. Law and J. Smart, *Proc. Royal. Soc.* **318**, 231 (1970).
22. C. J. Coombes, *J. Phys. F* **2**, 441 (1972).
23. S. J. Peppiatt and J. R. Sambles, *Proc. Royal. Soc.* **A345**, 387 (1975).
24. M. Rahman, *Micron* **13**, 273 (1982).
25. G. L. Allen, W. W. Gile and W. A. Jesser, *Acta. Metall.* **28**, 1695 (1980).
26. Ph. Buffat and J. P. Borel, *Phys. Rev.* **A13**, 2287 (1976).
27. P. R. Couchman and W. A. Jesser, *Phil. Mag.* **35**, 787 (1977).
28. Semchenko, V. K. (1961) In *Surface Phenomena in Metals and Alloys*, Pergamon Press, 281.
29. R. Kofman, P. Cheyssac and R. Garrigos, *Phase Transitions* **24-26**, 283 (1990).
30. G. L. Allen, W. W. Gill and W. A. Jesser, *Acta. Metall.* **28**, 1695 (1980).
31. G. D. T. Spiller, *Phil. Mag* **A46**, 535 (1982).
32. J. J. Metois and J. C. Heyraud, *J. Phys. France* **50**, 3175 (1983).
33. Dages, J., Gleiter, H. and Perepezko, J. H. (1986) *Mater. Res. Soc. Symp. Proc.* **57**.

34. C. J. Rossouw and S. E. Donnelly, *Phys. Rev. Lett.* **55**, 2960 (1985).
35. R. Goswami and K. Chattopadhyay, *Mater. Sci. Engg A179/180*, 198 (1994).
36. S. J. Peppiat, *Proc. Roy. Soc. A345*, 401 (1975).
37. P. Cheyssac, R. Kofman and R. Garrigos, *Physica Scripta* **38**, 164 (1988).
38. R. Goswami and K. Chattopadhyay, *Acta Metall. Mater.* **43**, 2837 (1995).
39. R. Goswami and K. Chattopadhyay, *Phil. Mag. Lett.* **68**, 215 (1993).
40. R. Goswami and K. Chattopadhyay, *Acta Metall. Mater.* **42**, 383 (1994).
41. F. Spaepen and D. Turnbull, *Scripta Metall.* **13**, 149 (1979).
42. A. K. Malhotra and D. C. Van Aken, *Phil. Mag A71*, 949 (1995).
43. K. S. Dubey and P. Ramachandra Rao, *Acta Metall.* **32**, 91 (1984).
44. H. Saka, Y. Nishikawa and T. Imura, *Phil. Mag. A57*, 895 (1988).
45. K. Sasaki and H. Saka, *Phil. Mag. A53*, 1207 (1991).
46. L. Graback and J. Bohr, *Phys. Rev. Lett.* **64**, 934 (1990).
47. D. L. Zhang and B. Cantor, *Acta Metall. Mater.* **39**, 1591 (1991).
48. J. D. Hoffman, *J. Chem. Phys.* **29**, 1192 (1958).
49. K. I. Moore, K. Chattopadhyay and B. Cantor, *Proc. Royal. Soc.* **414**, 499 (1987).
50. W. T. Kim and B. Cantor, *Acta Metall. Mater.* **40**, 3339 (1992).
51. R. Goswami and K. Chattopadhyay, *Appl. Phys. Lett.* **69**, 1 (1996).
52. Goswami, R. and Chattopadhyay, K. Unpublished work.
53. H. Gleiter, *Progress in Materials Science* **33**, 223 (1989).
54. H. W. Sheng, G. Ren, L. M. Peng, Z. Q. Hu and K. Lu, *Phil. Mag. Lett.* **73**, 179 (1996).
55. Massalski, T. B. (1982) Ed. *Binary Alloy Phase Diagram*. ASM, Metals Park.
56. K. I. Moore, D. L. Zhang and B. Cantor, *Acta Metall. Mater.* **38**, 1327 (1990).
57. D. L. Zhang, J. L. Hutchinson and B. Cantor, *J. Mater. Sci.* **29**, 2147 (1994).
58. D. L. Zhang, K. Chattopadhyay and B. Cantor, *J. Mater. Sci.* **26**, 1531 (1991).
59. D. L. Zhang and B. Cantor, *Acta Metall. Mater.* **40**, 2951 (1992).
60. D. L. Zhang and B. Cantor, *Philos. Mag. A62*, 557 (1990).

## Nanocomposite microstructure in a melt spun Al-Cu-Zr alloy

Dheepa Srinivasan and K. Chattopadhyay  
Department of Metallurgy  
Indian Institute of Science  
Bangalore 560 012  
India

**Key words:** nanocomposite, solid solution, intermetallic, eutectic

### Abstract

Rapid solidification of a ternary Al-Cu-Zr alloy results in a nanocomposite microstructure. In this study, melt spinning a  $\text{Al}_{82}\text{Cu}_{15}\text{Zr}_3$  alloy has resulted in the combined occurrence of, (a)  $0.5\ \mu\text{m}$  sized grains of Al solid solution and (b) fine grains (10-20 nm) of intermetallic  $\text{Al}_2\text{Cu}$  ( $\theta$ ) and  $\alpha$ -Al, along side each other. The larger  $\alpha$ -Al grains contain nanometric GP zones, with the Zr addition resulting in a grain refinement. In the other type of microstructure Zr promotes simultaneous nucleation of nanosized grains of the two equilibrium phases,  $\text{Al}_2\text{Cu}$  and  $\alpha$ -Al. Both these lead to a very high hardness of  $\sim 540$  VHN for this alloy and can be used as a candidate for a high strength alloy with good ductility at a low strain rate.

### Introduction

Production of fine grained stable two phase microstructures is central to superplastic forming. Although controlled hotworking was the preferred processing route for a long time, the recent developments in solidification processing opened up new avenues for synthesizing fine grained microstructures. The formation of aluminium based metallic glasses and their devitrification to nanoscaled crystalline structures, offers new possibilities for synthesizing multiphase nanostructured materials [1-5]. Here, the addition of minor alloying elements of rare earth and transition metal elements such as lanthanum, cesium, yttrium and notably zirconium, promote the amorphisation. The thermal stability of these glasses is closely related to their respective crystallization temperatures. Devitrification in these glasses often leads to a nanoscaled microstructure consisting of both stable and metastable phases. The latter affects the limit of operating stability by undergoing transformation to the equilibrium phases. It is possible in principle to produce the nanoscaled multiphase microstructure directly from the melt by controlling the nucleation and growth kinetics of the crystalline solids during the solidification process. We have already reported successful application of the above strategy to produce a nanocrystalline composite of  $\text{Ti}_2\text{Ni}$  phase in a TiNi matrix [6]. The basic principle behind these attempts is based on the fact that it is often possible under rapid solidification conditions, to suppress the heterogeneous nucleation and growth of phases at low undercoolings. In many systems a high undercooling promotes significantly higher nucleation rates of the solid product phase, with homogenous nucleation at the extreme end. The microstructure and phase selection in that case is nucleation controlled and results in a very fine microstructure. Often minor additions of ternary alloying elements have a pronounced effect in promoting such microstructures. The attention to such nucleation controlled microstructures which are distinct from well known growth controlled microstructures (such as dendritic and eutectic morphologies), is being given only recently. The Al-Cu near eutectic alloys in hot worked form are traditionally used by the superplastic community as an ideal model material for investigation. We have therefore attempted to probe the possibility of synthesizing nucleation controlled fine grained microstructures in

The grains measured  $\sim 0.5 \mu\text{m}$  in size and showed single crystal diffraction patterns characteristic of the fcc structure of  $\alpha\text{-Al}$  phase with a lattice parameter of  $\sim 4.05 \text{ \AA}$ . This was found to be in agreement with the lattice parameter measured using X-ray diffraction. The grains were all randomly oriented indicating no particular preferred direction during the growth of this phase from the liquid. A typical  $[011]$  zone is shown in Fig. 1b. The SADP's from these grains show pronounced streaking along  $\langle 100 \rangle$  directions, suggesting the possibility of formation of GP zones along this direction. One can also occasionally see a very diffuse ring passing through the (200) reflection of the aluminum solid solution. No other stable or metastable phases involving Al, Cu and Zr could be observed in these regions. A Bright field-Dark field pair of a grain at a higher magnification using the  $\alpha\text{-aluminum}$  (111) reflection is shown in Fig. 2. The grain boundaries show a rough and jagged morphology. This is typical of a highly perturbed growth interface which subsequently did not get enough time to equilibrate. This morphology clearly suggests growth in a highly undercooled melt. Further, considering that we are dealing with a concentrated alloy with a very high solute content of Cu and Zr, the microstructure clearly points to a nonequilibrium solute trapping process. The clusters of Cu atoms that go to form as GP zones are most likely to have formed as an outcome of solid state reaction, as a transient phase during cooling, subsequent to solidification.

Similar single phase granular microstructures have been observed earlier [12,14,15] in binary Al-Cu systems under different rapid solidification conditions. In all these observations however, the supersaturated grains measure at least  $5 \mu\text{m}$ 's. Whereas in this study the maximum  $\alpha\text{-Al}$  size observed is  $\sim 1/2 \mu\text{m}$ , the grain refinement brought about by the ternary Zr additions. Here the Zr could also be expected to aid the nucleation of grains of  $\alpha\text{-Al}$  by the suppression of other competitive phases.

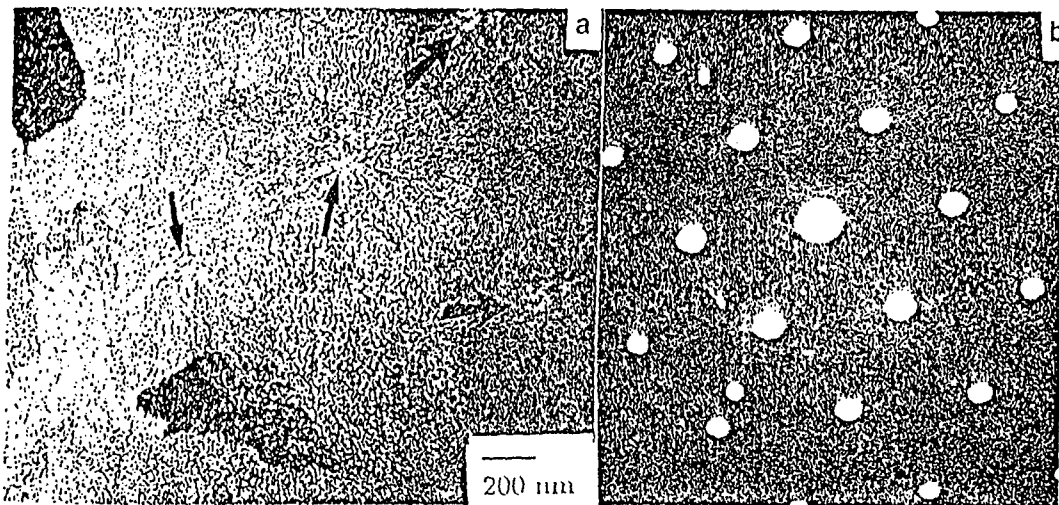


Fig. 1(a): Representative micrograph from the melt spun  $\text{Al}_{82}\text{Cu}_{15}\text{Zr}_3$  alloy revealing a granular microstructure made of Al solid solution, (b) Diffraction pattern from a grain along  $[011]$ . Streaking along  $\langle 001 \rangle$  seen due to GP zone formation.

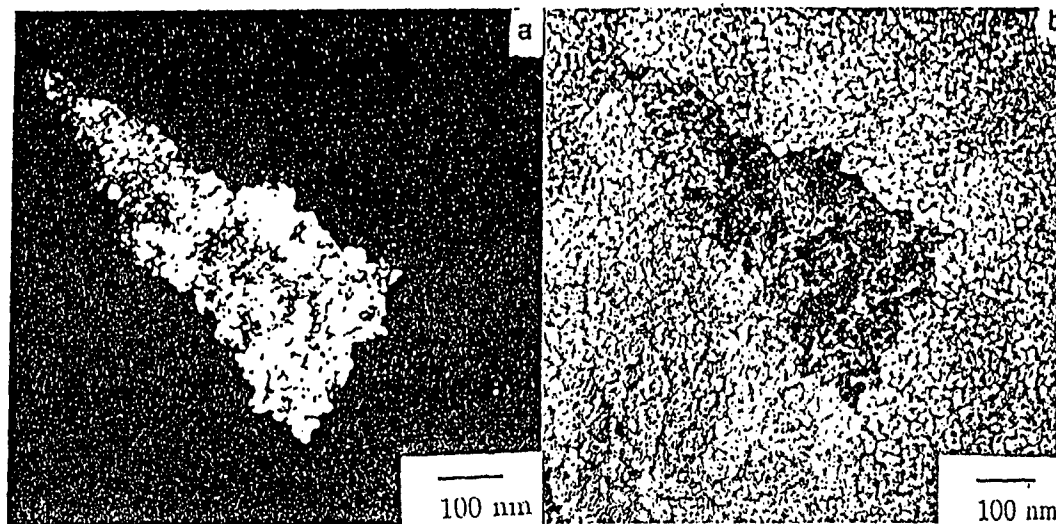


Fig 2 : (a) Dark field electron micrograph using a  $(11\bar{1})$  reflection showing an  $\alpha$ -Al grain diffracting. The grain is seen with re-entrant grain boundaries characteristic of solute trapping during solidification. (b) The corresponding bright field image, absorption contrast from the solutes seen in the adjoining grains

The second type of microstructure is distinctly different from that described above. This region comprises of very fine grains (10-20 nm) of  $\alpha$ -Al and  $\text{Al}_2\text{Cu}$  ( $\theta$ ) phases (Fig. 3a). Diffraction patterns show polycrystalline rings corresponding to both the phases, occurring together (Fig. 3b). The combined presence of fine grains of intermetallic  $\text{Al}_2\text{Cu}$  and  $\alpha$ -Al was further confirmed from DF images taken using rings of both phases. Fig. 3c is a representative DF image taken using overlapping rings,  $(11\bar{1})$  of  $\alpha$ -Al and  $(112)$  of  $\text{Al}_2\text{Cu}$ , revealing crystallites of both phases diffracting. A rough estimate of the volume fraction of these two phases indicate ~50% occupancy for the  $\text{Al}_2\text{Cu}$  phase and this coincides with the value obtained from the equilibrium binary diagram (which predicts volume fractions of ~48% using the lever rule). Similar microstructures are not reported in the rapidly solidified binary Al-Cu alloys and clearly points to a vital role of Zr in promoting competitive nucleation of both the phases.

The pathway of microstructure selection has clearly shifted from the nucleation of only  $\alpha$ -aluminum in the undercooled melt and its subsequent rapid growth (during which nonequilibrium trapping of Cu and Zr took place), to a competitive nucleation of both  $\alpha$ -aluminum and  $\text{Al}_2\text{Cu}$  at a very high rate yielding a nanometric two phase microstructure. The absence of any Zr containing phase also suggests that it has partitioned into both the phases. It is clear that the second type of microstructure is of great potential for developing, as solidified superplastic alloys. The fine grain and the high solute content will promote very high strength. In order to get an idea of the strength some preliminary hardness measurements have been carried out. A hardness of  $540 \pm 40$  VHN was measured for this alloy. The binary Al-17 at.% Cu alloy processed under similar conditions measured a hardness of  $120 \pm 20$  VHN. This phenomenally high value in the hardness is attributed to the nanoscaled microstructure (second type) as well as due to the trapped solutes of Zr and Al (in grains of  $\alpha$ -Al, first type).

It is of interest to see whether at low strain rates this alloy will give a higher elongation due to the fine grain sizes. This and the question of stability requires further investigation and work is in progress towards this direction.

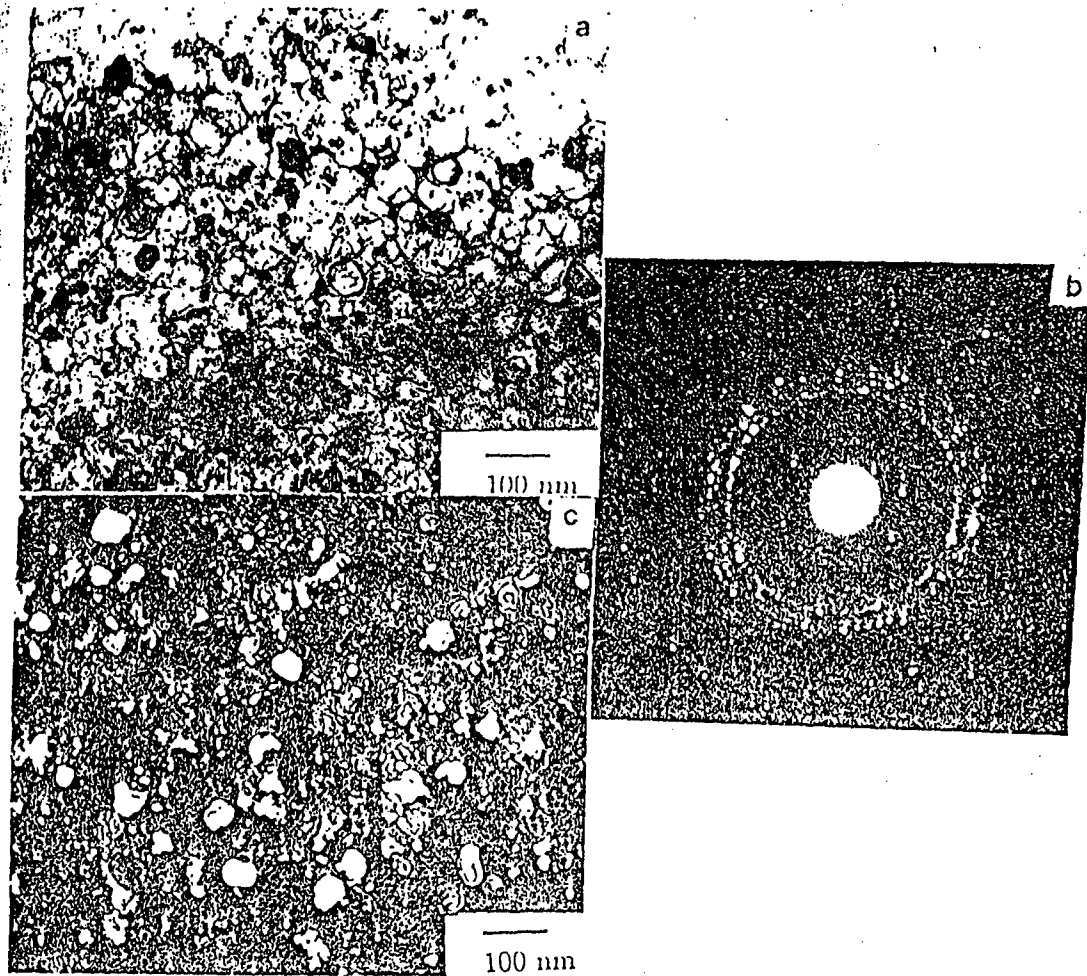


Fig. 3 : The second type of microstructure that occurred in the foils. Nearly equiaxed nano scaled grains of  $\alpha$ -Al and  $\text{Al}_2\text{Cu}$ , (b) Corresponding diffraction patterns showing polycrystalline rings of both the phases, (c) Dark field image using two overlapping rings,  $(111)_{\alpha\text{-Al}}$  and  $(112)_{\text{Al}_2\text{Cu}}$ , revealing the presence of fine grains of both phases.

### Conclusions

Melt spinning of the ternary  $\text{Al}_{82}\text{Cu}_{15}\text{Zr}_3$  alloy results in a nanocomposite exhibiting a very high hardness of  $\sim 540$  VHN. Two types of distinct microstructures have been observed. (a) Grains of Al solid solution ( $\sim 0.5 \mu\text{m}$ ) with solutes of both Cu and Zr trapped and, (b) nano scaled grains (10-20 nm) of intermetallic  $\text{Al}_2\text{Cu}$  and  $\alpha$ -Al, the two equilibrium phases. Both these account for the high hardness measured for this alloy. The present study opens up ideas for further investigations to synthesize such nanometric microstructures of the equilibrium phases directly from the liquid. However, this has to be followed by a detailed analysis to check out its thermal stability.

### Acknowledgments

The support for this work comes from AOARD, United States Air Force under contract No. F49620-95-1-0105.

### References

1. A. Inoue, M. Yamamoto, H.M. Kimura and T. Masumoto, *J. Mater. Sci., Lett.*, **6**, 194 (1987).
2. A. Inoue, K. Othera, A.P. Tsai and T. Masumoto, *Jpn. J. Appl. Phys.*, **27**, 279 (1988).
3. A. Inoue, K. Othera and A.P. Tsai, *Jpn. J. Appl. Phys.*, **27**, L 280 (1988a).
4. A. Inoue, K. Othera and T. Masumoto, *Jpn. J. Appl. Phys.*, **27**, 736 (1988b).
5. Y.H. Kim, A. Inoue and T. Masumoto, *Mater. Trans. JIM.*, **31**, 747 (1990).
6. R. Nagarajan and K. Chattopadhyay, *Acta Metall. et Mater.*, **42**, 947 (1994).
7. H.K. Hardy and T.J. Teal, *Prog. Metal Phys.*, **5**, 143 (1954).
8. A. Guinier, *Solid St. Phys.*, **9**, 294 (1959).
9. A. Kelly and R.B. Nicholson, *Prog. Mat. Sci.*, **10**, 151 (1962).
10. R.B. Nicholson and J. Nutting, *Phil. Mag.*, **3**, 531 (1958).
11. D.B. Williams and J.W. Eddington, *J. Mater. Sci.*, **12**, 126 (1977).
12. P. Ramachandra Rao, M. Laridjani and R.W. Cahn, *Z. Metallk.*, **63**, 43 (1972).
13. R.K. Singh, K. Chattopadhyay, S. Lele and T.R. Anantharaman, *J. Mater. Sci.*, **17**, 1617 (1982).
14. M.G. Scott and J.A. Leake, *Acta Metall.*, **23**, 503 (1975).
15. S.C. Gill and W. Kurz, *Acta Metall. Mater.*, **41**, 3563 (1993).
16. H.A. Davies and J.B. Hull, *Scripta Met.*, **6**, 241 (1972).

# Formation and Coarsening of a Nanodispersed Microstructure in Melt Spun Al-Ni-Zr Alloy

Dheepa Srinivasan and K. Chattopadhyay  
Department of Metallurgy  
Indian Institute of Science  
Bangalore 560 012

## 1. Introduction

There have been numerous reports on the enhanced mechanical properties in aluminium based nanocrystalline alloys [1-9]. However the high temperature properties often suffer due to rapid coarsening. Design of nanocrystalline alloys, therefore, demand an attention into issues of microstructural stability. Alloying additions which promote dispersions of second phase with low interfacial energy may hold promise in this direction. In this context Zr serves as an excellent candidate in the development of nanocrystalline aluminium alloys. In ternary alloys with small amounts of Zr (< 1 at%), the transition metal addition promotes glass formation and inhibits the growth of crystalline phases. The decrease in mass transport provides opportunities for reducing the scale of the microstructure. Supersaturated dilute alloys of Al with Zr have been found to precipitate out a coherent metastable  $Al_3Zr$  phase [2-9]. By virtue of the small lattice misfit between the precipitate and the Al matrix and the low values of solubility as well as diffusivity of Zr in Al, this phase has been found to resist coarsening even upto temperatures as high as 723K [ 2-10 ] Thus a judicious combination of chemistry and processing conditions can yield nanocrystalline composite structures that are stable against coarsening.

With the above aim in view, we explore in this paper, the microstructural development of a rapidly solidified  $Al_{89}Ni_{10}Zr_1$  alloy and its subsequent decomposition behaviour at elevated temperatures in order to asses the possibility of developing stable high strength nanostructured aluminium alloys.

## 2. Experimental Details

A ternary  $Al_{89}Ni_{10}Zr_1$  alloy was prepared by induction melting high purity (>99.999%) elemental mixtures. The alloy was rapidly solidified using the melt spinning technique on to a rotating Cu wheel with a wheel surface velocity of 45 m/s. The thermal stability of the alloy was evaluated by aging at four different temperatures (423K, 523K, 623K and 723K) for various times. The microstructure was examined by transmission electron microscopy (JEOL 2000 FX II, 200KV). Thin foils for microscopy were prepared using a GATAN duo ion mill, using Ar ions, with a sputtering angle ranging from 10-15°. Vickers microhardness measurements were made at a load of 10 g using a Shimadzu HMV 2000 microhardness tester.

### 3. Experimental Observations

#### (i) The initial microstructure

The melt spun alloy comprised predominantly of grains ( $\sim 500$ - $600$  nm in size) of Al solid solution (Fig. 1a), interrupted occasionally by a eutectic microstructure, made up of  $\text{Al}_3\text{Ni}$  rods ( $\sim 20$ - $30$  nm) in an  $\alpha$ -Al matrix, grown in a coupled manner (Fig. 1b). SADP's from the  $\alpha$ -Al grains also reveal the presence of a faint ring close to the  $(200)_{\text{Al}}$  reflection, along with a single crystal Al pattern. This is seen as a diffuse ring corresponding to the strongest reflection (131) of  $\text{Al}_3\text{Ni}$ , indicating the presence of very fine particles of some other Ni rich phase, trapped in the interdendritic region, during rapid quenching.

A variation in the observed microstructure is the occurrence of primary  $\text{Al}_3\text{Ni}$  particles ( $150$  -  $200$  nm) (arrowed) surrounded by the fine eutectic microstructure. No particular orientation relationship was found between the two eutectic phases. The as spun microstructure was then broken up with a view to obtaining an uniformly dispersed nanocomposite microstructure.

#### (ii) Low temperature aging : A nanodispersed microstructure

At temperatures of  $423\text{K}$  and  $523\text{K}$  annealing for short times (upto  $1\text{h}$ ) results in an uniform distribution of  $\text{Al}_3\text{Ni}$  dispersoids in an  $\alpha$ -Al matrix (Fig. 2). However, it was difficult to identify a particular region as having originated from either the single phase region or the rod eutectic grains, of the as spun microstructure. The eutectic rods broke into fine grains of  $\text{Al}_3\text{Ni}$  in an  $\alpha$ -Al matrix, whereas in regions with Al solid solution the interdendritic phase grew into  $\text{Al}_3\text{Ni}$  dispersoids of similar sizes. The nanosized distribution was almost uniform in the sample. However, in some regions the  $\text{Al}_3\text{Ni}$  dispersoids were stacked along a line (such as that arrowed in Fig. 2a), while some others showed the presence of coarser  $\text{Al}_3\text{Ni}$  particles (Fig. 2b) in an otherwise uniform microstructure (inset). The former kind indicates a Raleigh like instability occurring along these rods, while the latter larger  $\text{Al}_3\text{Ni}$  particles imply that these were regions with pre-existing primary  $\text{Al}_3\text{Ni}$  in the as spun structure. The fine  $\text{Al}_3\text{Ni}$  dispersoids displayed a spherical morphology and exhibited no orientation relationship with the Al matrix, following the as solidified random orientation. No other Zr containing phase could be seen after low temperature aging.

Annealing was performed at higher temperatures to check the stability of this microstructure.

#### (iii) High temperature aging : The Precipitation of Zr

Prolonged aging at low temperatures ( $> 2$  hrs) as well as annealing for short times at higher temperatures ( $623\text{K}$  and  $723\text{K}$ ) results in the coarsening of the nanosized intermetallic  $\text{Al}_3\text{Ni}$  phase. This is shown in the DF images in Fig. 3, taken using  $\text{Al}_3\text{Ni}$  and  $\alpha$ -Al reflections respectively. At these higher temperatures longer aging times ( $> 1\text{h}$  at  $623\text{K}$  and  $> 15\text{min}$  at  $723\text{K}$ ) not only lead to a coarsening of the two eutectic phases, but also to the precipitation of fine dispersions of a cubic  $\text{Al}_3\text{Zr}$  phase (Fig. 4). This is a metastable phase, the equilibrium phase being one with a tetragonal structure. This cubic phase is seen to precipitate out of both  $\alpha$ -Al and  $\text{Al}_3\text{Ni}$  grains indicating that Zr was accommodated in both the eutectic phases on rapid quenching. Electron diffraction patterns (insets) identify this to be the cubic  $\text{Al}_3\text{Zr}$  having an  $L1_2$  structure, with the occurrence of extra superlattice reflections indicative of ordering, along with the fundamental ones.

The Al<sub>3</sub>Zr precipitates share a cube on cube orientation relationship with the  $\alpha$ -Al grains. The orientation relationship between the orthorhombic (DO<sub>20</sub>) Al<sub>3</sub>Ni and the ordered fcc (L1<sub>2</sub>) Al<sub>3</sub>Zr precipitate has been established as :

$$[112]_{\text{Al}_3\text{Zr}} // [111]_{\text{Al}_3\text{Ni}} ; (111)_{\text{Al}_3\text{Zr}} // (110)_{\text{Al}_3\text{Ni}}$$

This OR is reflected in the SADP and the stereogram in Figs. 5a and 5b respectively. This OR prescribes 8 variants, four of which can be identified in the dark field image in Fig. 4b (numbered).

No nucleation of or transformation to the equilibrium Al<sub>3</sub>Zr phase was observed even after long aging times (upto 16 hrs) at these elevated temperatures.

#### (iv) Coarsening of Al<sub>3</sub>Zr

The metastable phase retains its fine sizes even after long aging times, when present in the  $\alpha$ -Al grains (Fig. 4a). However, the Al<sub>3</sub>Zr particles coarsen significantly when present in the Al<sub>3</sub>Ni grains, going from ~ 5 nm (15 min) to nearly 50 nm (8 hrs). This difference in the sizes of the precipitates in the two matrices is illustrated in the DF images in Fig. 4, after the same time (8 h) and temperature of aging (723 K). Since there is negligible coarsening observed in the  $\alpha$ -Al grains, subsequent coarsening data were plotted and considered only for the precipitate particles present in the Al<sub>3</sub>Ni matrices.

There is a significant difference in the sizes of the precipitates present within the grains and those along the grain boundary. The average starting sizes of the grain boundary precipitates are larger (10-20 nm) than those within the grain (0-10 nm). Fig. 5 shows comparative histograms of the size distributions of the Al<sub>3</sub>Zr particles in the grain boundaries and the grain interiors as a function of aging time (723 K). This shows the anticipated 3 step behavior, starting with nucleation, followed by growth and coarsening. Initially there is a nucleation of these precipitate particles taking place (for 5 and 15 min) and most of the particles lie in the lower range (Fig. 5a and 5b). At one hour of aging (Fig. 5c), there is a simultaneous process of nucleation and growth taking place, with effect that the particles inside the grain grow from an average size of 0-10 nm to 10-20 nm. Whereas along the boundary, even though there is growth taking place leading to an increase in the density of particles in the 10-20 nm range, the numbers in the lower (0-10 nm) range are higher. This is indicative of pinning of smaller matrix precipitates by the migrating boundary thereby resulting in the presence of a number of smaller particles. This is illustrated in Fig. 6.

Subsequent to this aging results in a coarsening taking place at the grain boundary and inside the grain. The average sizes now reach 60-70 nm for the GB precipitates and 30-40 nm for the ones inside the grain (Fig. 5d and 5e). This shows a decrease in the numbers in the lower size range and a corresponding increase in the numbers in the larger range. Here the grain boundary precipitates coarsen faster facilitated by the easy diffusion paths along the boundaries as compared to the matrix insides. The cumulative coarsening rates of the average particle size for the two cases are shown in Fig. 7.

The hardness of these alloys before and after annealing were determined to see the variation in this property on coarsening. Fig. 8 gives a plot of hardness measured after different aging times at the four heat treatment temperatures. The as spun alloy was found to have an average hardness of 400 VHN with some portions of the ribbon being as high as 500 VHN. On aging, for short times at low temperatures of 423K and 523K the average hardness is still quite high

(250 - 300 VHN), but is lower than that of the untreated sample. High temperature aging however, leads to coarsening of the phases and hence a significant decrease in the hardness values.

#### 4. Discussion

##### (i) The solidification sequence

The composition used in this work corresponds to a hypereutectic one in the corresponding binary system. The addition of 1 at% Zr will not alter the phase field significantly and the solidification structure of the ternary alloy will be of a similar nature to that of the binary, around this composition. This would be predominantly made of the two eutectic phases, either formed by a coupled growth or having first  $\text{Al}_3\text{Ni}$  nuclei as a primary phase followed by the eutectic rods. However, a very high quenching rate and hence a large undercooling can enable the direct nucleation of the  $\alpha$ -Al phase resulting in a single phase microstructure with segregates in the interdendritic regions [11]. These two above mentioned microstructures therefore, require substantially different rates of quenching.

In the present study, the occurrence of both these microstructures alongside each other, in a sample subject to a particular quenching rate suggests that the ternary transition metal (Zr) addition has played a significant role in the microstructure evolution. Here, Zr goes into solution and produces an effect equivalent to that achievable under high heat transfer conditions. Minor amounts of Zirconium acts to promote a high undercooling in some regions thereby resulting in the nucleation of the  $\alpha$ -Al grains in the same sample in which the eutectic microstructure is also present, both being subject to the same physical conditions of quenching rate etc, the latter requiring a comparatively lower undercooling.

Two striking observations of the present investigation are the feathery morphology of the grains of the  $\alpha$ -Al in the as spun state and the absence of any orientation relationship between the two eutectic phases on annealing. The presence of a diffuse ring corresponding to a Ni rich phase in the diffraction patterns as well as the appearance of a contrast within the grains leads to the conclusion of the presence of very fine interdendritic segregates of some other phase. Although no other additional diffraction effect could be observed from the  $\alpha$ -Al grains in this work, the origin of formation of such phases from the liquid in the interdendritic regions is documented in the binary Al-Ni alloy [11].

This also explains why no orientation relationship could be observed between the  $\text{Al}_3\text{Ni}$  dispersoids and the  $\alpha$ -Al grains, on annealing. Here, the already present, randomly oriented interdendritic phase serves as the nuclei for subsequent growth, on aging the  $\alpha$ -Al grains. The annealed microstructure therefore follows the random OR of the as spun phases. Whereas , regions with a coupled growth of alternate phases of Al and  $\text{Al}_3\text{Ni}$  undergo a Raleigh like instability leading to a pinching off of the eutectic rods resulting in a nanodispersed microstructure. Here again the original random orientation of the as spun phases manifest after annealing.

On the other hand, in the solid state it has been reported that the same eutectic phases share a single unique orientation, seen both when obtained as a directionally solidified product as well as a precipitation product [12, 13]. The  $\text{Al}_3\text{Ni}$  forms as plates when precipitated out of

supersaturated solutions as against the spherical morphology displayed by the dispersoids observed in the present study. This strongly emphasises the role played by elastic energy in both the growth morphology as well as the orientation relationship. However, it has been reported that the same eutectic phases have a unique orientation relationship and that  $\text{Al}_3\text{Ni}$  forms as plates [ 11 ] when precipitated out of supersaturated solutions. This implies that the eutectic phases do not share any particular orientation relationship when formed from the liquid governed only by the interfacial energy minimisation criteria. Whereas in the solid state both elastic as well as interfacial energies play a role in dictating the common orientation shared between them. Thus in this case, the decomposition of the metastable solid solution does not require any fresh nucleation and the  $\text{Al}_3\text{Ni}$  dispersoids inherit the orientation that they were quenched into.

**(ii) Coarsening :**

The appearance of the  $\text{Al}_3\text{Zr}$  phase as a precipitation product only after long time or at high temperatures can be understood in terms of the low value of diffusivity of Zr in Al. This indicates the high stability of Zr as a solute .

On high temperature aging it has been observed that there is a five fold increase in the sizes of both the  $\text{Al}_3\text{Ni}$  grains as well as the  $\text{Al}_3\text{Zr}$  that precipitated out of the  $\text{Al}_3\text{Ni}$  grains. In comparison the  $\text{Al}_3\text{Zr}$  particles present in the  $\alpha\text{-Al}$  grains do not grow so significantly during the aging process. This is by virtue of the small values of lattice misfit and hence the low energy coherent interfaces (they share a cube on cube orientation relationship) between them. In contrast the different crystal structures of  $\text{Al}_3\text{Zr}$  and  $\text{Al}_3\text{Ni}$  do not favour a low energy coherent interface between them. The absence of the equilibrium tetragonal  $\text{Al}_3\text{Zr}$  phase in this study confirms the stability of the metastable phase.

The coarsening behaviour of the  $\text{Al}_3\text{Zr}$  precipitates in the  $\text{Al}_3\text{Ni}$  grains is quite complex, as now it involves a simultaneous coarsening of the matrix phases as well as the precipitates and hence three species diffusing down the chemical potential gradient. When the  $\text{Al}_3\text{Ni}$  grain grows it needs more Ni diffusing from the surroundings. Similarly when an  $\alpha\text{-Al}$  grain grows, the excess Ni must be driven away to regions that are depleted of Ni. Coarsening studies on the Al- $\text{Al}_3\text{Ni}$  eutectic have mainly been on the stability of  $\text{Al}_3\text{Ni}$  rods in an Al matrix, and here no preferential different rates of coarsening have been observed for the two phases. Whereas in the present study when the  $\text{Al}_3\text{Ni}$  grains grow from  $< 10$  nm to nearly  $1 \mu\text{m}$  in the same time in which the  $\alpha\text{-Al}$  grains remain the same, it is clear that there is some additional aspect that governs the coarsening behaviour of these phases in the ternary system. It is expected that the precipitate particles play a dominant role in this by way of the vastly different coarsening behaviour that they exhibit in both the grains. The higher degree of coarsening of the  $\text{Al}_3\text{Ni}$  grains is probably due to the lack of coherent/semi coherent interface boundaries as in the  $\alpha\text{-Al}$  grains.

The high hardness values of this alloy indicate a possibility of developing very high strength alloys. This high value is attributed to a Hall-Petch type of strengthening as well as a solid solution type strengthening brought about respectively by the microstructure made of fine eutectic rods of intermetallic  $\text{Al}_3\text{Ni}$  and Al, and grains of  $\alpha\text{-Al}$  with trapped solute in the interdendritic regions. The low temperature heat treatment yield a fine and uniform dispersion of nanometric  $\text{Al}_3\text{Ni}$  in an  $\alpha\text{-Al}$  matrix, with the added Zr still trapped in both the phases. This displays nearly the same strength as that of the as spun alloy. However, here one expects

a greater ductility. The nanocomposites obtained via this route can have a significant potential applications.

## 5. Conclusions

A nanodispersed microstructure of Al<sub>3</sub>Ni particles in an  $\alpha$ -Al matrix was obtained after low temperature annealing of the melt spun alloy. Both, the as spun alloy as well as the one after low temperature heat treatment showed high hardness values (~ 500 VHN), brought about by the nanoscaled microstructure and the trapped solute. Whereas at high temperatures precipitation and coarsening lead to a lower hardness. No equilibrium tetragonal phase was observed. The orientation relationship between the precipitate and the matrices has been established. The metastable Al<sub>3</sub>Zr phase coarsens considerably when present in the Al<sub>3</sub>Ni matrix compared to the low coarsening rate in an  $\alpha$ -Al matrix.

## Acknowledgements

This work has received support from AOARD, United States Air Force, contract No.

## References

1. D.G. Morris and M.A. Morris, Acta Metall. 39, 1793 (1991).
2. H. Nagahawa, K. Othara, K. Higashi, A. Inoue and T. Masumoto, Phil. Mag. Lett. 67, 225 (1993).
3. M.N. Rittner, J.A. Eastman and J.R. Weertman, Scripta Metall. 31, 841
4. N. Ryum, Acta Metall. 17, 269 (1994).
5. O. Izumi and D. Oelschlagel, Scripta Metall. 3, 619 (1969).
6. E. Nes, Acta Metall. 20, 499 (1972).
7. M.S. Zedalis and M.E. Fine, Met. Trans. 17A, 2189 (1986).
8. Y.C. Chen, M.E. Fine, J.R. Weertman and R.E. Lewis, Scripta Metall. 21, 1003 (1987).
9. S.C. Chung, S.Z. Han, H.M. Lee and H.S. Hwon, Scripta Metall. 33, 687 (1995).
10. V.R. Parameswaran, J.R. Weertman and M.E. Fine, Scripta Metall. 23, 147 (1990).
11. K. Chattopadhyay Phd Thesis, Banaras Hindu University, (1978).
12. F.D. Lemkey, R.W. Hertzberg and J.A. Ford, Trans of the Met. Soc. of AIME, 233, 334 (1965)
13. H.B. Smartt and T.H. Courtney, Met. Trans: , 3, 2000 (1972)

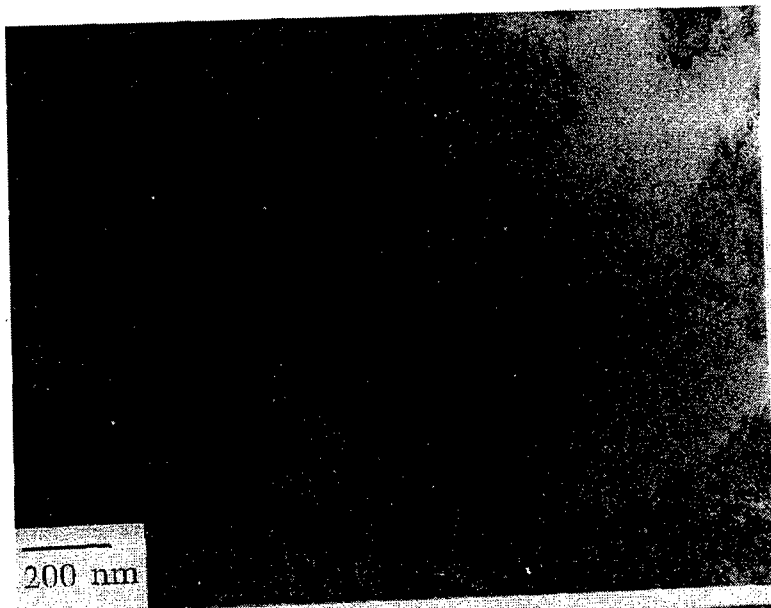


**Fig.1a**



**Fig.1b**



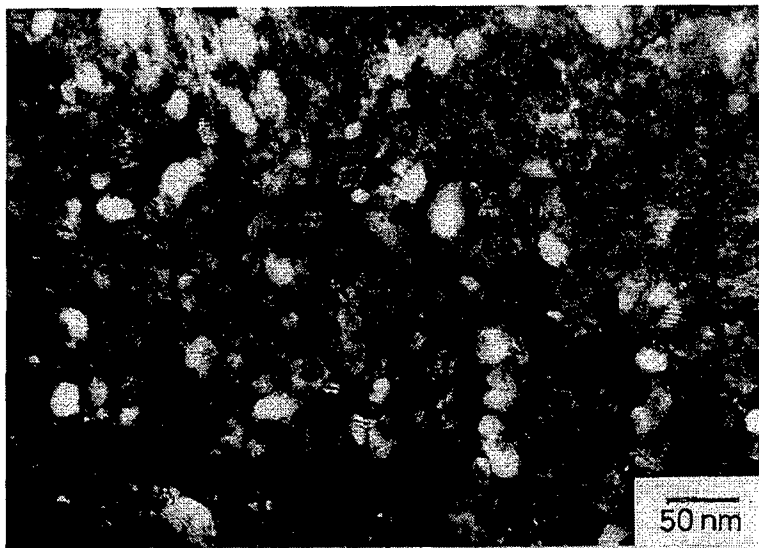


**Fig.2a**

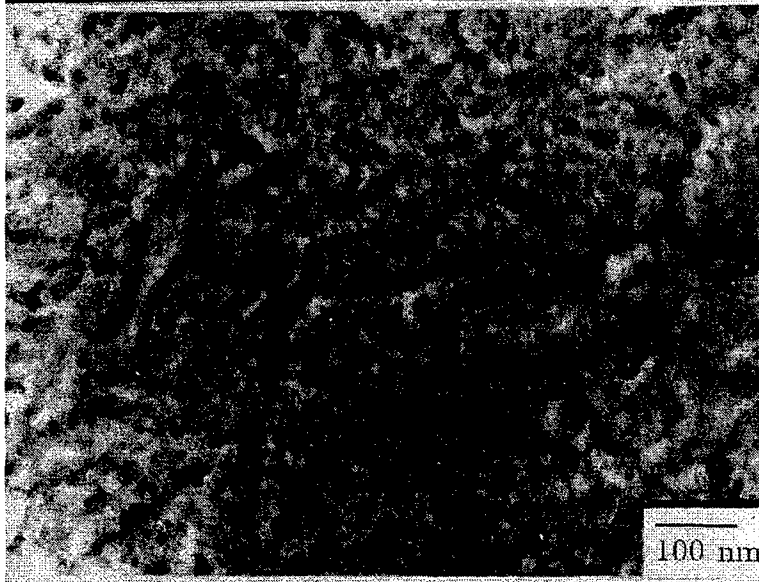


**Fig.2b**



**Fig.2c**

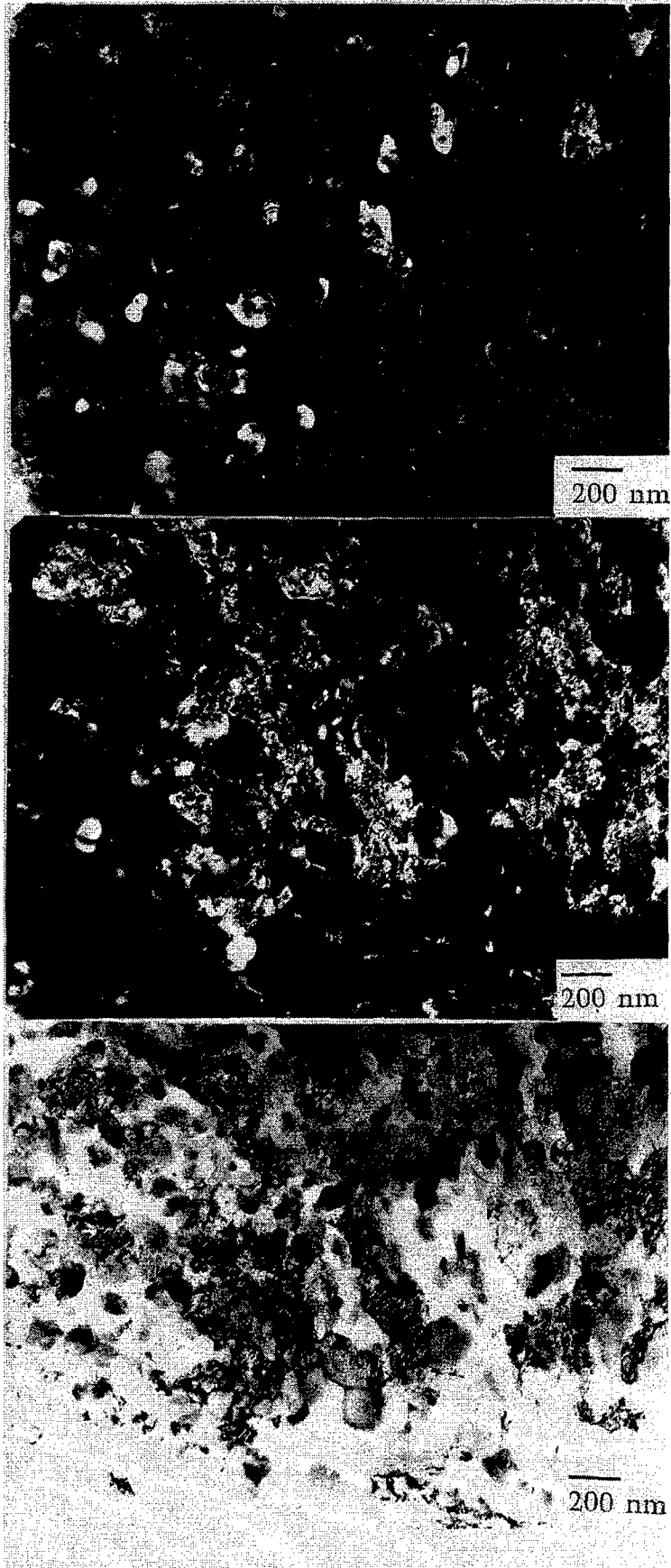


Fig.3



Fig.4



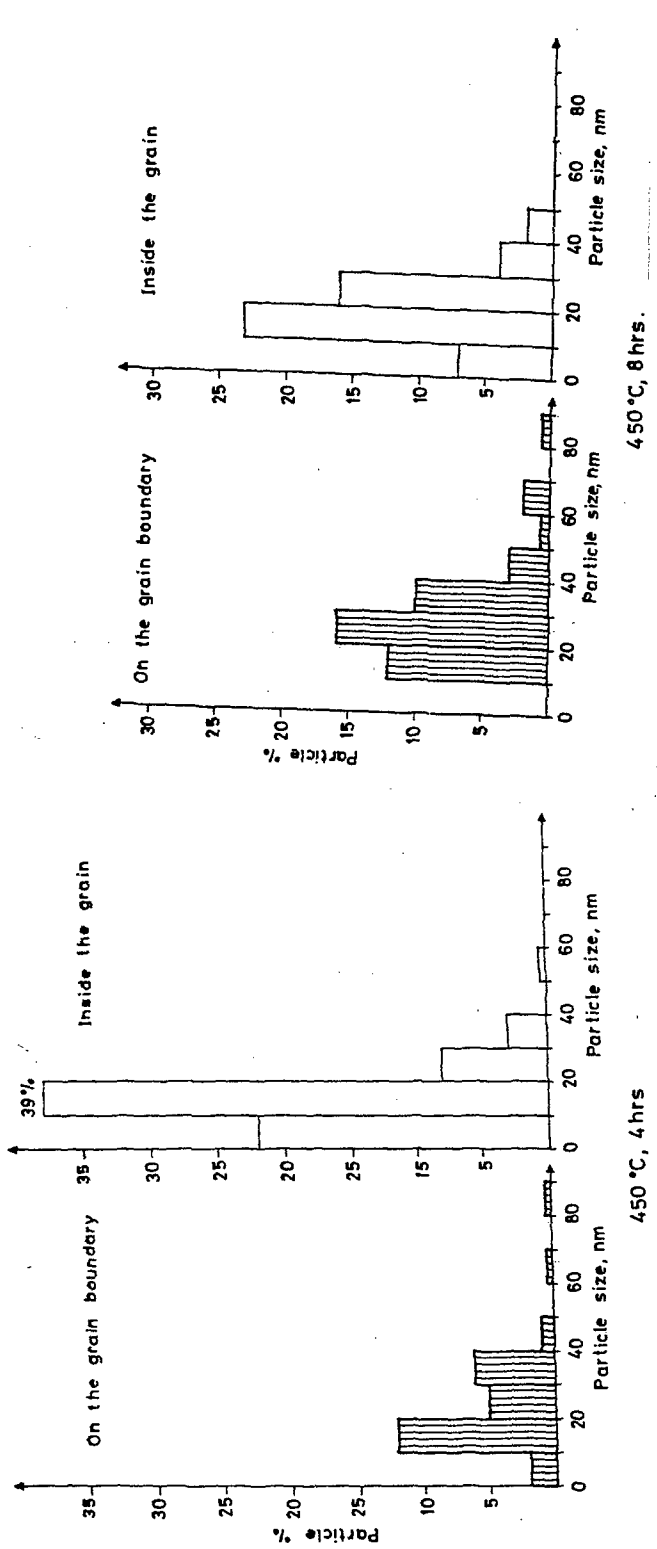
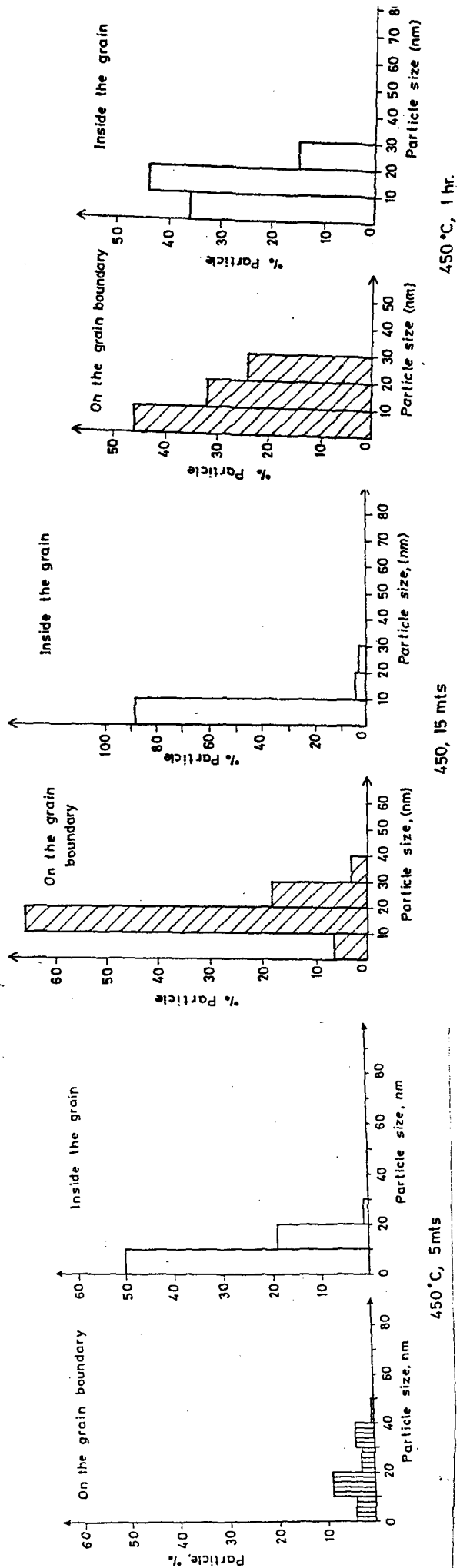


Fig.6



Fig.7

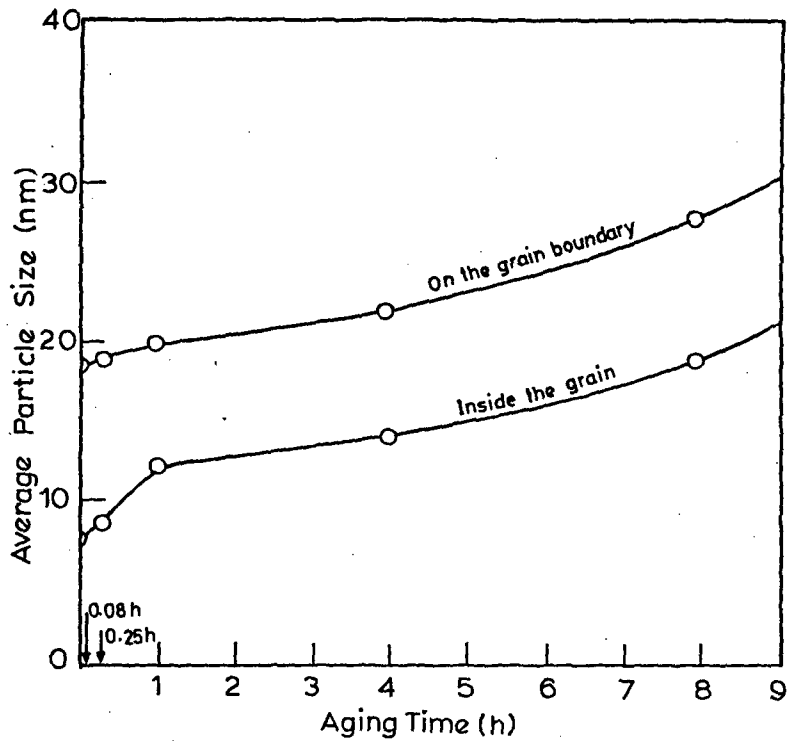


Fig.8

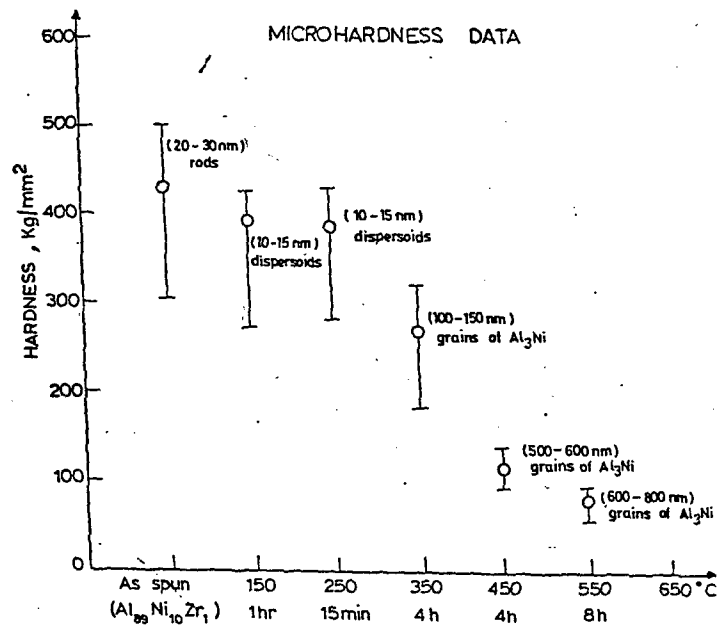


Fig.9